ACCEPTED FOR PUBLICATION IN THE ASTROPHYSICAL JOURNAL SUPPLEMENT SERIES
Preprint typeset using LaTeX style emulateapj v. 5/2/11

SPECTROSCOPIC SURVEY OF G AND K DWARFS IN THE *HIPPARCOS* CATALOG. I. COMPARISON BETWEEN THE *HIPPARCOS* AND PHOTOMETRIC PARALLAXES

BOKYOUNG KIM[1], DEOKKEUN AN[1,2], JOHN R. STAUFFER[2,3], YOUNG SUN LEE[4],
DONALD M. TERNDRUP[2,5], JENNIFER A. JOHNSON[5]

Accepted for Publication in the Astrophysical Journal Supplement Series

ABSTRACT

The tension between the *Hipparcos* parallax of the Pleiades and other independent distance estimates continues even after the new reduction of the *Hipparcos* astrometric data and the development of a new geometric distance measurement for the cluster. A short Pleiades distance from the *Hipparcos* parallax predicts a number of stars in the solar neighborhood that are sub-luminous at a given photospheric abundance. We test this hypothesis using spectroscopic abundances for a subset of stars in the *Hipparcos* catalog, which occupy the same region as the Pleiades in the color-magnitude diagram. We derive stellar parameters for 170 nearby G and K type field dwarfs in the *Hipparcos* catalog based on high-resolution spectra obtained using KPNO 4-m echelle spectrograph. Our analysis shows that, when the *Hipparcos* parallaxes are adopted, most of our sample stars follow empirical color-magnitude relations. A small fraction of stars are too faint compared to main-sequence fitting relations by $\Delta M_V \gtrsim 0.3$ mag, but the differences are marginal at a 2σ level partly due to relatively large parallax errors. On the other hand, we find that photometric distances of stars showing signatures of youth as determined from lithium absorption line strengths and $R'_{\rm HK}$ chromospheric activity indices are consistent with the *Hipparcos* parallaxes. Our result is contradictory to a suggestion that the Pleiades distance from main-sequence fitting is significantly altered by stellar activity and/or the young age of its stars, and provides an additional supporting evidence for the long distance scale of the Pleiades.

Subject headings: solar neighborhood — stars: abundances — stars: distances — open clusters and associations: individual (the Pleiades)

1. INTRODUCTION

The determination of accurate distances to stars is the key to understanding how stars and the Galaxy have formed and evolved. The *Hipparcos* mission (Perryman et al. 1997) was especially valuable, providing trigonometric parallaxes for $\sim 10^5$ stars to a precision of 1–2 mas. Therefore, it was a big surprise when the *Hipparcos* distance to the Pleiades open cluster was in disagreement with distances from the main-sequence (MS) fitting at more than a 3σ level (Pinsonneault et al. 1998). To reconcile a short Pleiades from *Hipparcos*, it has been suggested that the metal abundance of the Pleiades is significantly lower than the solar (Percival et al. 2003), thereby decreasing a distance from MS fitting. However, there are a large number of spectroscopic studies on the cluster's metallicity in the literature, which essentially indicate a near-solar metallicity of the cluster (see references in An et al. 2007b). In addition, the enhanced helium abundance of the cluster was suggested (Belikov et al. 1998), but the expected amount of helium has to be enormous ($Y \approx 0.34$) in this solar metallicity cluster. An argument was also made that distance estimates from theoretical stellar models have been overestimated for young clusters due to yet unknown, age-related physics (van Leeuwen 1999).

The discrepant *Hipparcos* result for the Pleiades has subsequently led to many efforts to determine the cluster's distance from binaries and independent parallax measurements (e.g., Munari et al. 2004; Pan et al. 2004; Soderblom et al. 2005). These results confirm the long distance scale from MS fitting, supporting the hypothesis that the *Hipparcos* result was in error. The most likely explanation is related to the *Hipparcos* parallaxes themselves. Pinsonneault et al. (1998) showed that a dozen bright stars near the center of the Pleiades all had virtually the same parallax (~ 9 mas), which is more than 1 mas larger than the mean parallax for other cluster stars. They attributed this to a local zero-point error of individual stellar parallaxes that are correlated over the *Hipparcos*' 0.9 deg field of view (see also Narayanan & Gould 1999). By re-reducing part of the *Hipparcos* data, Makarov (2002, 2003) were able to demonstrate that such correlated errors could explain the discrepant Pleiades parallax estimate. Additional effects may result from the way the *Hipparcos* data were obtained and analyzed (van Leeuwen 2005; van Leeuwen & Fantino 2005), and it was hoped that a new reduction of the *Hipparcos* raw data might resolve the issue.

However, the new reduction of the *Hipparcos* data (van Leeuwen 2007a,b) still leads to a short distance to the Pleiades. In the most recent analysis, van Leeuwen (2009) found 8.32 ± 0.13 mas for the average parallax of the Pleiades, or $(m-M)_0 = 5.40 \pm 0.03$ (120.2 ± 1.9 pc), which is significantly shorter than the weighted average distance $(m-M)_0 = 5.63 \pm 0.02$ (133.7 ± 1.2 pc) from independent astrometric and binary solutions (see references in An et al. 2007b). Moreover, Melis et al. (2014) recently used the Very Long Baseline Interferometry (VLBI) to directly measure a geometric distance to the Pleiades, and found $(m-M)_0 = 5.67 \pm 0.02$ (136.2 ± 1.2 pc), which agrees with the long distance scale.

[1] Department of Science Education, Ewha Womans University, 52 Ewhayeodae-gil, Seodaemun-gu, Seoul 03760, Republic of Korea; deokkeun@ewha.ac.kr
[2] Visiting astronomer, Kitt Peak National Observatory, National Optical Astronomy Observatory, which is operated by the Association of Universities for Research in Astronomy (AURA) under a cooperative agreement with the National Science Foundation.
[3] Spitzer Science Center, California Institute of Technology, Pasadena, CA 91125
[4] Department of Astronomy and Space Science, Chungnam National University, 99 Daehak-ro, Daejeon 34134, Republic of Korea
[5] Department of Astronomy, The Ohio State University, 140 West 18th Avenue, Columbus, OH 43210

An alternative, but indirect test of the Pleiades distance can be made by examining nearby field stars that occupy the same region on a color-magnitude diagram (CMD) as those in the Pleiades. The short *Hipparcos* distance to the Pleiades predicts a number of stars in the solar neighborhood that are subluminous at a given photospheric abundance. Since absolute magnitudes (M_V) of stars are sensitive to the photospheric abundance, it is possible to distinguish sub-luminous stars (with the hypothesized Pleiades-like phenomenon) from normal ones, when accurate metallicity measurements are available. Here, our core assumption in this paper is that parallaxes for the majority of stars in the *Hipparcos* catalog are correct, but only a small fraction of these stars (such as those in the Pleiades) have incorrect parallaxes due to large, hidden systematic errors.

Previously, Soderblom et al. (1998) performed such test using a set of nearby field stars, but found no stars of similar characteristics with the Pleiades members. However, the interpretation of their result is somewhat complicated by the fact that stars in their sample mostly have spectral types later than K2. Late-type, young, chromospherically active stars can be heavily spotted and hence variable, and their optical colors can differ significantly from those of older field stars of the same spectral type (Stauffer et al. 2003). On the other hand, rapid rotation does not cause significant photometric anomalies of stars with spectral types earlier than K2.

The goal of this paper is to obtain accurate metal abundances for a subset of G and early K-type stars in the *Hipparcos* catalog, and look for sub-luminous field stars at a given metallicity. Such stars will have longer distances from MS fitting than those computed from the *Hipparcos* parallaxes. Furthermore, if the assertion by van Leeuwen (2009) is correct, and the young age of the Pleiades is responsible for the long MS-fitting distance to the cluster, young field stars, such as those selected from strong lithium absorptions or Ca II H and K emissions, will be fainter than older counterparts by $\Delta M_V \gtrsim 0.2$ mag at a common [Fe/H]. Assuming a constant star formation rate and an age of ~ 8 Gyr for the thin disk stellar population (e.g., see Casagrande et al. 2016, and references therein), about 2.5% of stars in the solar neighborhood were formed in the last ~ 200 Myr. A couple of young stars should be present in a sample of ~ 100 field stars. The expected number of such stars will decrease if an exponentially decreasing star formation rate is assumed (e.g., Aumer & Binney 2009), but a relatively large number of young open clusters in the solar neighborhood implies the presence of many young stars near the Sun. Furthermore, a vertical age gradient in the disk (e.g., Casagrande et al. 2016) would yield more young stars near the Galactic plane. A well-defined set of field stars can be used to disprove a null hypothesis that the short distance to the Pleiades is caused by the young age of the cluster.

This paper is organized as follows. In § 2 we describe spectroscopic observations and data reductions. Derivation of stellar parameter is given in § 3. In § 4 we derive MS-fitting distances for individual stars using spectroscopic metallicities, and compare them to the *Hipparcos* parallaxes. A summary of our results is given in § 5.

2. SPECTROSCOPIC OBSERVATIONS AND DATA REDUCTIONS

2.1. *Sample Selection*

The top left-hand panel in Figure 1 illustrates our sample selection based on a $B-V$ CMD. Grey points are stars with good parallaxes ($\sigma_\pi/\pi \leq 0.07$) in the revised *Hipparcos* catalog (van Leeuwen 2007a,b). We took *BV* photometry of these stars from the NASA Star and Exoplanet Database (NStED), most of which are those transformed from $B_T V_T$ in the Tycho-2 catalog (Høg et al. 2000) using transformation equations found in Mamajek et al. (2002, 2006). We neglected foreground extinctions of these stars since they are mostly found within ~ 50 pc from the Sun.

The parallelogram in the top left-hand panel of Figure 1 indicates our color-magnitude selection, corresponding to $4.74 \leq M_V \leq 6.34$ at $B-V = 0.60$ and $6.86 \leq M_V \leq 8.46$ at $B-V = 1.0$. The bluer color limit was set to minimize the evolutionary effect on stellar luminosity and to perform a reliable line absorption analysis. We selected stars near or below the MS of the Pleiades on the absolute V magnitude (M_V) versus $B-V$ CMD, assuming a distance of the cluster from the recent *Hipparcos* parallax, $(m-M)_0 = 5.40$ (van Leeuwen 2009). We retained stars if they are found within $\Delta M_V \sim 1.4$ mag below and $\Delta M_V \sim 0.2$ mag above the MS of the Pleiades, as shown by the top and the bottom sides of the parallelogram. We applied a color limit $B-V = 1.0$ to exclude chromospherically active low-mass stars with large color anomalies (Stauffer et al. 2003).

In the top left-hand panel of Figure 1, the thick solid line represents the observed MS of the Hyades (Pinsonneault et al. 2004). We adopted a distance to the cluster's center of mass $(m-M)_0 = 3.33 \pm 0.01$ from the *Hipparcos* catalog (Perryman et al. 1998). The Hyades covers a large area on the sky, which makes parallax measurements of its individual members less vulnerable to the suspected spatial correlation of the *Hipparcos* parallax (Pinsonneault et al. 1998; Narayanan & Gould 1999; de Bruijne et al. 2001). The cluster is approximately 550 Myr old (Perryman et al. 1998), and has $[Fe/H] = +0.13 \pm 0.01$ (Paulson et al. 2003) with negligible foreground reddening (e.g., Taylor 1980). The two thin solid lines are 550 Myr old theoretical models at $[Fe/H] = -0.3$ and $[Fe/H] = 0.0$ (An et al. 2007b), of which colors were calibrated using the observed MS of the Hyades. All together, these lines show a typical metallicity sensitivity of colors and magnitudes of MS stars. In this study, however, we avoided using theoretical isochrones and relied on the observed MS of the Hyades to empirically derive a MS-fitting distance to individual field stars.

Meanwhile, the top side of the parallelogram in Figure 1 is not exactly parallel to the solar metallicity isochrone. This is because the Pleiades' MS, which was used to set our sample color-magnitude cut, is known to become progressively fainter than those for older stars or standard stellar models as one moves toward redder colors (Stauffer et al. 2003; An et al. 2007b), although the observed magnitude offset in the $T_{\rm eff}$ range of our sample is not as severe as those seen for stars with $B-V \gtrsim 1$ (see Figure 20 in An et al. 2007b). Nevertheless, our search for anomalously faint stars in the solar neighborhood is almost insensitive to how we set the upper limit in stellar brightness since such stars would be significantly fainter than the above brightness limit in any case (see discussions in § 4.2).

In total 480 G- and K-type dwarfs satisfy the above selection criteria. We combined V-band magnitude with K_s in the Two Micron All Sky Survey (2MASS; Skrutskie et al.

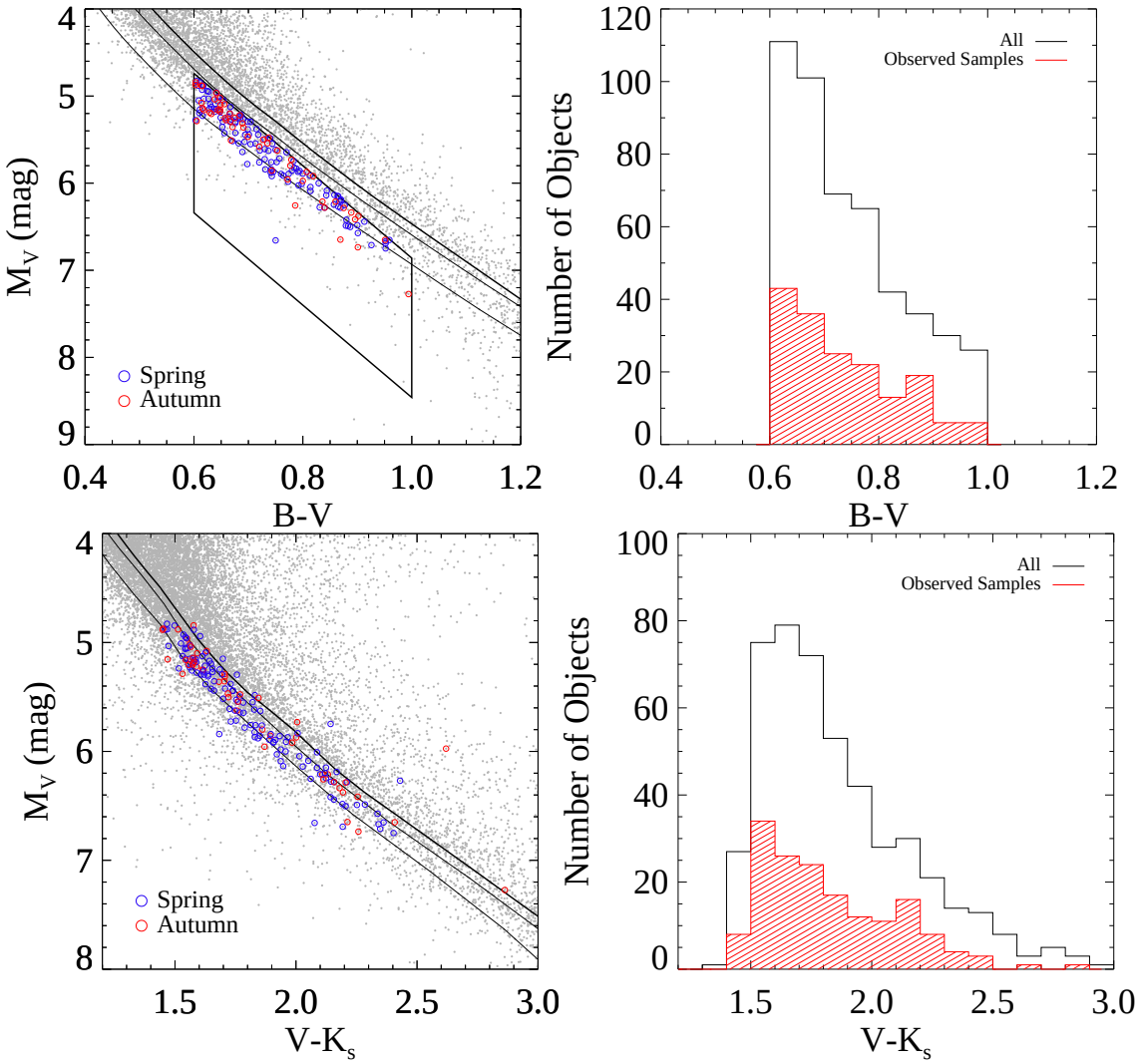

FIG. 1.— *Top left:* Color-magnitude diagram of field stars in the solar neighborhood with *Hipparcos* parallaxes ($\sigma_\pi/\pi \leq 0.07$). The parallelogram represents a color-magnitude selection of spectroscopic targets in this study, where the KPNO samples observed in the spring (N = 120) and autumn (N = 53) runs are shown in blue and red circles, respectively. The thick solid line is the observed MS of the Hyades ([Fe/H]= +0.13) at the *Hipparcos* distance to the cluster (Perryman et al. 1998), while thin lines are theoretical isochrones with empirical colors at [Fe/H]= –0.3 and 0.0, respectively (An et al. 2015). *Bottom left:* Same as in the top left-hand panel, but with $V - K_s$ colors. *Right panels:* Color distributions of the KPNO sample stars (red histogram) in $B - V$ (top) and $V - K_s$ (bottom), respectively. The black histogram represents a distribution of all stars in the *Hipparcos* catalog ($\sigma_\pi/\pi \leq 0.07$) that are found within the parallelogram in the top left-hand panel.

2006)[6]. Except five stars (HIP 9172, HIP 56837, HIP 91438, HIP 96100, and HIP 101997), our targets have valid K_s-band measurements, which are not saturated, undetected, blended, or contaminated. The bottom left-hand panel in Figure 1 shows the same set of stars in the $V - K_s$ CMD, although we did not employ $V - K_s$ colors in our sample selection.

2.2. *Observations and Data Reductions*

We selected a random subset of *Hipparcos* field stars, which satisfy our color-magnitude cut, and obtained their high-resolution ($\lambda/\Delta\lambda \sim 60{,}000$) spectra with the echelle spectrograph on the Mayall 4-m telescope at Kitt Peak National Observatory (KPNO). Most of our targets are bright ($V \sim 9$ mag), and are spread all around sky, except those with low declinations ($\delta \lesssim -30°$) due to observing restrictions at KPNO. Our observing campaign was composed of 5 nights in May 2010 and 4 nights in September 2010. In the left-hand panels of Figure 1, targets observed in spring and autumn are marked in blue and red circles, respectively. Unresolved binaries are cooler than single stars and therefore better represented in $V - K_s$ with its longer wavelength baseline. Our color-magnitude cut is likely smeared out in the $V - K_s$ CMD by these unresolved binaries along with photometric color errors. The $B - V$ and $V - K_s$ color distributions of our observed sample are shown by a red shaded histogram in the right-hand panels in Figure 1. The open histogram represents a distribution of the initial sample selected above from the *Hipparcos* catalog (those within a parallelogram in the top left-hand panel). The overall shapes of the red shaded and open histograms in each panel are similar with each other, as expected from a random selection of stars in our spectroscopic observations.

The sky was clear in spring, but the dome was closed during

[6] This publication makes use of data products from the Two Micron All Sky Survey, which is a joint project of the University of Massachusetts and the Infrared Processing and Analysis Center/California Institute of Technology, funded by the National Aeronautics and Space Administration and the National Science Foundation.

two nights in autumn due to bad weather conditions. We used a red long camera and settled on the 58.5-63 grating with a $\sim 1''$ slit width. With the 2048×2048 T2KB CCD and 226-1 cross disperser, the wavelength coverages were set to 4340 Å–7670 Å in May, and 4400 Å–7870 Å in September. The spectra are of high quality, with high signal-to-noise (S/N) ratios (> 100 per pixel).

In total 120 stars were observed in spring, and 53 stars were observed in autumn. Three stars were observed in both spring and autumn runs (HIP 113884, HIP 104733, HIP 98792). From our observing runs, spectra for 170 field stars in the *Hipparcos* catalog were obtained. Table 1 lists our sample stars with V, $B-V$, and $V-K_s$ colors and their errors from the *Hipparcos* catalog. A minimum error in V and $B-V$ was set to 0.02 mag. The 9^{th} and 10^{th} columns show revised *Hipparcos* parallaxes (π) and their errors (van Leeuwen 2007a,b). The M_V and its error in the next two columns were computed using V and π and their associated errors. Seven targets were identified as a spectroscopic binary system in the 10^{th} catalogue of spectroscopic binary orbits (Pourbaix et al. 2004)[7], and are marked in Table 1. A number of repeat observations for each target is indicated in the following columns. About one third of the sample stars (N = 69) were observed 2–3 times, and 8 stars were observed in two different nights to check for systematics in our abundance measurements.

We reduced raw data frames using standard data processing packages in IRAF[8]. This included a bias correction, bad pixel correction, wavelength calibration using Th-Ar lamp, spectral extraction, and radial velocity correction. For data taken in autumn, we found a uniformly increasing bias pattern toward one side of the CCD, which consistently appeared over the entire observing run. We combined all of the zero-exposure frames, made an average bias frame, and subtracted it from our science data frames. We corrected for a wavelength shift from a line-of-sight velocity using the Hα line profile. When the Hα line was not available, the Na I 5890.0 Å line was used for a radial velocity correction.

3. DERIVATION OF STELLAR PARAMETERS

Our conclusions about stars with the *Hipparcos* parallaxes are sensitive to the adopted sizes of errors in metallicity, while stellar parameters – effective temperatures ($T_{\rm eff}$), surface gravity ($\log g$), and metallicity ([Fe/H]) – derived from spectroscopy are subject to various systematic errors. Since such errors could originate from different spectroscopic analysis techniques (e.g., Torres et al. 2012), we derived stellar parameters in two parallel approaches. We employed a spectral synthesis code MOOG[9] (Sneden 1973) based on equivalent width (EW) measurements of iron lines (§ 3.1). Because this procedure was performed by hand, we restricted our MOOG analysis to a subset of stars in the sample (N = 74 out of 170) with highly precise parallax measurements ($\sigma_\pi/\pi \leq 0.03$), and those (N = 13) having largest M_V differences between *Hipparcos* and MS fitting despite their less accurate parallaxes ($\sigma_\pi/\pi > 0.03$). For the entire sample (including those analyzed using MOOG), we employed an automated spectral matching technique (SMT), which iteratively fits synthetic spectra to an observed spectrum to search for the best matching parameters with least human intervention. For an efficient estimation of stellar parameters with SMT, we degraded our spectra to a medium resolution ($R = 10,000$), while keeping the same precision in the stellar parameter estimates. Below we describe each of these two approaches, along with external checks with previous work in the literature.

3.1. *Stellar Parameters from MOOG*

We selected stars with accurate parallaxes ($\sigma_\pi/\pi \leq 0.03$) in our sample (N = 74), and used MOOG to derive their precise atmospheric parameters, taking advantage of high-resolution ($R \sim 60,000$) spectra of high quality (S/N > 100). We selected a list of Fe lines, which were commonly included in both Bensby et al. (2003) and Boesgaard et al. (2013). Within the wavelength range of our echelle data, there were 37 Fe I lines and 5 Fe II lines. These lines are listed in Table 3 along with their central wavelengths, excitation potentials (E.P.), and oscillator strengths ($\log gf$). We determined a local continuum for each absorption line using a polynomial with a degree of 3, and measured its EW using SPECTRE[10] (Sneden, version 2003).

We constructed Kurucz stellar model atmospheres based on newly computed opacity distribution functions (ODFs) with updated opacities and abundances (Castelli & Kurucz 2004)[11]. We interpolated ODFs at a given set of [Fe/H] and microturbulence ξ, and constructed desired models using the ATLAS9 code of stellar atmosphere. We assumed solar abundance ratios in Grevesse & Sauval (1999) with an enhancement in the α-elements ratios (O, Mg, Si, Ca, and Ti) relative to Fe: +0.4 for [Fe/H] ≤ -1.0, +0.3 for [Fe/H] = –0.75, +0.2 for [Fe/H] = –0.5, +0.1 for [Fe/H] = –0.25, and 0.0 for [Fe/H] $\geq +0.0$.

We used the *abfind* driver in MOOG to constrain $T_{\rm eff}$, $\log g$, [Fe/H], and micro-turbulence (ξ), self-consistently. The effective temperature was derived by requiring that individual line abundances be independent of excitation potential and that ξ be independent of line strength. Insisting on ionization equilibrium between Fe I and Fe II allowed for a simultaneous determination of $\log g$ with $T_{\rm eff}$ and ξ. Our sample stars are relatively cool, and therefore non-LTE corrections are likely negligible (see Bensby et al. 2014).

Table 2 lists $T_{\rm eff}$, $\log g$, [Fe/H], and ξ of stars analyzed using MOOG. In addition to 74 stars with accurate parallax measurements, we included 13 stars in our MOOG analysis, which show large differences in distance between *Hipparcos* and MS fitting (see § 4.2). We adopted a solar Fe abundance A(Fe)[12]= 7.52 in Anders & Grevesse (1989). The [Fe/H]$_{\rm corr}$ is a corrected [Fe/H] value, which was put on the metallicity scale adopted in this paper, and is described below in detail. We computed an error in [Fe/H] by propagating errors in Fe I and Fe II abundances. If there exist repeat measurements ($N_{\rm obs}$), we took a standard deviation of these measurements divided by a square root of $N_{\rm obs}$ or the one propagated from individual abundance errors, whichever is larger. A typical root-mean-square (rms) dispersion of Fe I abundance is approximately 0.15 dex for each star. Given the large number of iron lines used in this study (N = 37), this results in an unrealistically small error in [Fe/H] ($\sigma \approx 0.02$ dex). To estimate more realistic errors in abundance, we ran additional models with

[7] `http://sb9.astro.ulb.ac.be`

[8] IRAF is distributed by National Optical Astronomy Observatories (NOAO), which is operated by the Association of Universities for Research in Astronomy, Inc., under arrangement with the National Science Foundation, United States.

[9] http://www.as.utexas.edu/∼chris/moog.html

[10] http://www.as.utexas.edu/∼chris/spectre.html

[11] http://kurucz.harvard.edu/grids.html

[12] $A({\rm Fe}) \equiv \log[N({\rm Fe})/N({\rm H})] + 12$.

different input stellar parameters ($\Delta T_{\rm eff}$ = ±100 K, $\Delta \log g$ = ±0.3 dex, Δ[Fe/H] = ±0.1 dex, and $\Delta\xi$ by ±0.3 km s^{-1}). Table 4 shows mean abundance errors obtained from all stars analyzed using MOOG. A quadrature sum of these errors yields a systematic error in [Fe/H] of the order of 0.08 dex.

For an external check on our derived stellar parameters, we compared our values with atmospheric parameters for a large number of field dwarfs in Valenti & Fischer (2005, hereafter VF05). They used a software package Spectroscopy Made Easy (SME; Valenti & Piskunov 1996) to derive $T_{\rm eff}$, $\log g$, and individual elemental abundances based on high-resolution spectra. They obtained both an overall metallicity ([M/H]) and an elemental abundance of iron ([Fe/H]) for each star, but we utilized their [Fe/H] as we derived metallicities using MOOG from EW measurements of Fe.

Figure 2 shows comparisons in $T_{\rm eff}$ (top), $\log g$ (middle), and [Fe/H] (bottom) between MOOG and VF05. Statistical properties of the parameter comparisons are summarized in the first row in Table 5. The MOOG $T_{\rm eff}$ is on average 53 K higher than VF05 $T_{\rm eff}$, which is not unexpected from the two independent analyses. However, our spectroscopic $\log g$ estimates are systematically smaller than those from VF05. The observed trend in $\log g$ is similar to those seen from a large number of disk stars in Bensby et al. (2014), who found that $\log g$ determinations from Fe I and Fe II ionization equilibrium are systematically smaller than the one based on the *Hipparcos* parallax. The offset was seen for dwarfs over a wide range of temperature in their study, but there was no convincing trend observed for giants. Theoretical models (An et al. 2007b, 2015) also suggest that MS stars within a narrow range of color ($0.6 \leq B-V \leq 1.0$) have surface gravities $4.4 \lesssim \log g \lesssim 4.6$ over a range of metallicity covered by our sample stars, but our MOOG estimates are about 0.3 dex smaller than these. Nevertheless, the $\log g$ dependence of our metallicity estimate from MOOG is weak (Table 4), and an adjustment of $\log g$ would hardly affect our [Fe/H] estimates.

In Figure 2 observed 1σ dispersions in the parameter comparisons are $\sigma(\Delta T_{\rm eff})$ = 104 K and $\sigma(\Delta$[Fe/H]) = 0.06. VF05 computed formal 1σ uncertainties of their parameter estimates as $\sigma(T_{\rm eff})$ = 44 K and σ([Fe/H]) = 0.03, suggesting that $T_{\rm eff}$ and [Fe/H] determined from our MOOG analysis have a precision of $\sigma(T_{\rm eff}) \approx 90$ K and σ([Fe/H]) ≈ 0.05 dex. The latter is close to our expectation ($\sigma \approx 0.08$ dex) from errors computed by varying stellar input parameters in the models (Table 4).

We also checked the accuracy of stellar parameters derived using MOOG against a calibration sample in Casagrande et al. (2010), which have been used in the derivation of their empirical color-$T_{\rm eff}$ relations based on the Infrared Flux Method (IRFM). They provided a large compilation of stellar parameters from a high-resolution spectroscopy in the literature. We cross-identified stars in their and our catalogs based on both coordinates and V magnitudes. There were 9 stars in common, and the comparison with their stellar parameters is included in Table 5. The average difference in $T_{\rm eff}$ between Casagrande et al. (2010) and our MOOG-based estimates is 32 K.

Our [Fe/H] estimates from MOOG are systematically lower than those in VF05 and in Casagrande et al. (2010) by 0.07 ± 0.01 dex and 0.02 ± 0.01 dex, respectively. However, the above metallicity estimates from MOOG were not adjusted for an instrumental correction to the solar Fe abundance, because we did not obtain a solar spectrum during the observing runs. For this reason, we adjusted our original [Fe/H] estimates from MOOG to match published values in VF05 by adding a constant offset (Δ[Fe/H] = 0.07 dex). The last column ([Fe/H]$_{\rm corr}$) in Table 2 lists [Fe/H] values after this correction.

3.2. *Spectral Matching Technique (SMT)*

In addition to the EW analysis using MOOG, we employed a SMT to derive stellar parameters ($T_{\rm eff}$, $\log g$, and [Fe/H]) for all of our sample stars. The SMT routine is essentially a modified version of the NGS1 technique adopted in the SEGUE (Sloan Extension for Galactic Understanding and Exploration; Yanny et al. 2009) Stellar Parameter Pipeline (SSPP; Lee et al. 2008a,b). It was originally designed to match a grid of synthetic models to low-resolution stellar spectra in the Sloan Digital Sky Survey (SDSS; York et al. 2000; Stoughton et al. 2002). We modified and optimized the original NGS1 code to analyze our echelle spectra. We found that the accuracy of stellar parameters derived from SMT remains almost unaffected with varying spectral resolutions. For this reason, we linearly re-binned observed spectra with Gaussian smoothing to 0.25 Å per pixel ($R \approx 10,000$) for a fast and efficient analysis of our extensive data set. The smoothing was also helpful for improving S/N ratios of the spectra.

We generated a grid of models using the Kurucz stellar model atmospheres based on the new ODFs as described above. We utilized a pre-computed set of models[13] to construct a finer grid by linearly interpolating these models over a wide range of parameter space, covering 4000 K $< T_{\rm eff} <$ 10000 K in steps of 250 K, $0.0 < \log g < 5.0$ in steps of 0.25 dex, and $-5.0 <$ [Fe/H] $< +1.0$ in steps of 0.25 dex. Synthetic model spectra were then generated using the *synthe* code at 3,000 Å $\leq \lambda \leq$ 10,000 Å at a resolution of 0.01 Å, where we adopted ξ[km s^{-1}] = $-0.345 \times \log g + 2.22$, which was derived from the SSPP calibration with high-resolution spectra. After constructing a full set of synthetic spectra, we re-sampled model spectra to 0.25 Å wide linear pixels, corresponding to R = 10,000 at 5000 Å.

We matched synthetic spectra with observed data at 4500 Å $< \lambda <$ 5500 Å and 5900 Å $< \lambda <$ 6900 Å, which contain a large number of isolated Fe lines along with other various metallic lines. In each of the above wavelength ranges, we normalized model spectra using a pseudo-continuum, which was constructed by iteratively rejecting data points that are more than 1σ below and 4σ above a fitted polynomial curve. The degree of a polynomial was set to 21 to cover each echelle order. We took the same normalization step for the observed spectra, which produced the same level of line-strength suppression. We used the χ^2 minimization routine MPFIT[14] (Markwardt 2009) to search the grid of synthetic spectra for the best-fitting model parameters. In this step, we generated a synthetic spectrum at intermediate values of $T_{\rm eff}$, $\log g$, and [Fe/H] from the model grid using a spline interpolation. Errors in the best-fitting model parameters were determined by the square root of the diagonal elements in the covariance matrix.

Figure 3 shows an example of the results from SMT. The black solid line is an observed spectrum of HIP 98677 after downgrading its resolution to R = 10,000. The red

[13] Available at http://kurucz.harvard.edu/grids.html.
[14] http://www.physics.wisc.edu/∼craigm/idl/fitting.html

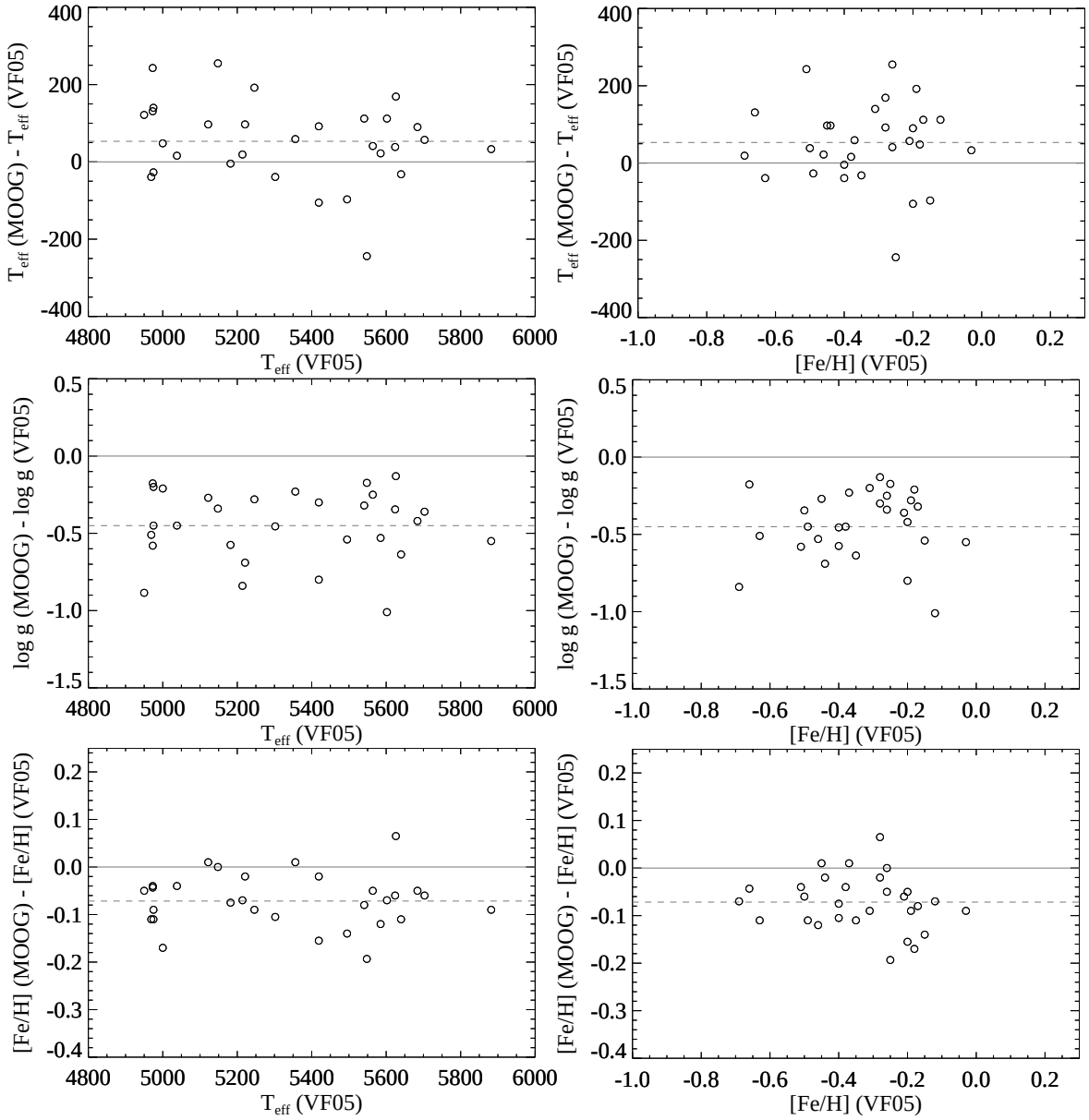

FIG. 2.— Comparisons in spectroscopic parameters between VF05 and MOOG. The dashed line indicates a mean difference, while the solid line is a zero difference. In the bottom panels, metallicities from MOOG represent raw estimates, before applying a zero-point adjustment (see text).

solid line represents our best-fitting synthetic spectrum with $T_{\rm eff}$ = 5519 K, $\log g$ = 4.56 dex, [Fe/H] = –0.24 dex, and ξ = 0.65 km s^{-1}, which shows an excellent match to the observed data. The second through 7$^{\rm th}$ columns in Table 6 summarize results from SMT with 1σ errors in $T_{\rm eff}$, $\log g$, and [Fe/H]. For stars observed multiple times, average values of individual parameter estimates are listed. Errors in these quantities are either random errors derived from SMT or a standard deviation of measurements from multiple observations divided by a square root of $N_{\rm obs}$, whichever is larger. The mean errors are 79 K, 0.097 dex, and 0.067 dex in $T_{\rm eff}$, $\log g$, and [Fe/H], respectively.

We repeated the above search for stellar parameters ($\log g$ and [Fe/H]) while holding $T_{\rm eff}$ fixed using the IRFM relation (Casagrande et al. 2010). We refer to this approach as SMT2 as opposed to SMT3 based on the full three-parameter fitting above. The polynomial equation in the IRFM relation includes metallicity terms, so we derived $T_{\rm eff}$ using $B-V$ photometry at an initial [Fe/H] derived above. The photometric temperature led to the new $\log g$ and [Fe/H] estimates. With these values, we took one more iteration to estimate photometric $T_{\rm eff}$ and found best-fitting metallicity and surface gravity for our target stars. The 9$^{\rm th}$ through 14$^{\rm th}$ columns in Table 6 show these values and their errors. The error in $T_{\rm eff}$ was computed assuming 0.02 mag error in the $B-V$ photometry. The typical errors in $T_{\rm eff}$, $\log g$, and [Fe/H] from this approach are 60 K, 0.020 dex, and 0.016 dex, respectively. As summarized in Table 5, SMT2 results are generally consistent with those from SMT3: Differences in the derived parameters are $\Delta T_{\rm eff}$ = 51 K, $\Delta \log g$ = 0.09, and Δ[Fe/H] = 0.03.

Comparisons of stellar parameters with MOOG are shown in Figures 4 and 5 for SMT3 and SMT2, respectively. In each panel, a solid line represents a zero difference, and a dashed line is an average difference between MOOG and SMT3/SMT2. Corrected values of [Fe/H] from MOOG were used in all comparisons. The SMT3 $T_{\rm eff}$ estimates are on

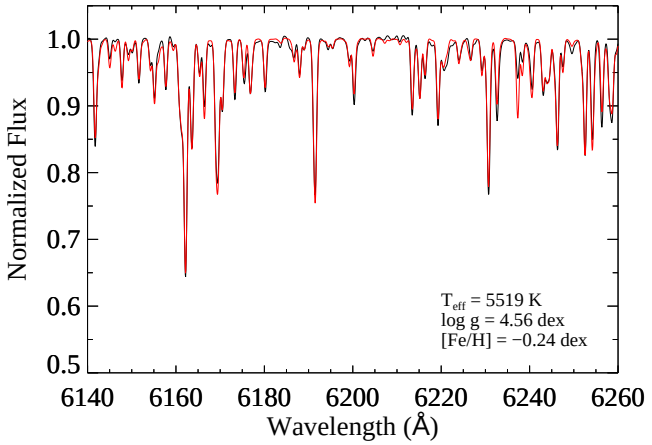

FIG. 3.— A segment of an observed spectrum of HIP 98677 (grey line). The red line represents the best-fitting synthetic model spectrum in the SMT analysis. The spectral resolution was degraded to $R \sim 10,000$ (see text).

average higher than those from MOOG, but the difference is small ($\Delta T_{\rm eff}$ = 37 K). Similarly, the MOOG $T_{\rm eff}$ estimates are higher than those from SMT2, but the average difference is negligible (19 K). As discussed above, $\log g$ values from MOOG were probably underestimated, and the comparison with SMT suggests that the difference in $\log g$ is correlated with its metallicity. The metallicities from both SMT3 and SMT2 are systematically higher than those from MOOG by Δ[Fe/H] = 0.09 dex and 0.05 dex, respectively.

Figure 6 displays comparisons in $T_{\rm eff}$, $\log g$, and [Fe/H] between SMT3 and VF05. The temperatures and metallicities from SMT3 are systematically higher than those from VF05 by $\Delta T_{\rm eff}$ = 85 K and Δ[Fe/H] = 0.07 dex (see Table 5). Given the correlation between the two quantities, it seems likely that a higher $T_{\rm eff}$ has led to a higher [Fe/H]. There also appears a correlation of the $\log g$ difference with metallicity, although the trend is much weaker than those seen from the comparisons of VF05 with MOOG.

The 1σ dispersion in $T_{\rm eff}$ comparison between SMT3 and VF05 is 95 K. This is consistent with a reported internal precision in each of the methods (44 K and 79 K for VF05 and SMT3, respectively). Similarly, a 1σ dispersion in $T_{\rm eff}$ comparison between SMT3 and MOOG is 101 K. This suggests that MOOG temperatures have internal errors of $\sim$ 90 K, and is consistent with our earlier estimate based on a comparison with VF05. Similarly, a 1σ dispersion in [Fe/H] comparison between SMT3 and VF05 is 0.06 dex, which is not far from a quadrature sum of individual internal precision measurements (0.030 dex for VF05 and 0.067 dex for SMT3). A 1σ dispersion in [Fe/H] comparison between SMT3 and MOOG is 0.08 dex, and is broadly consistent with σ([Fe/H]) = 0.05–0.08 for our MOOG results (see § 3.1).

In terms of a zero point in metallicity, all of the above comparisons suggest that metallicity estimates from SMT3 are about 0.1 dex higher than those from VF05. The level of the systematic offset is not alarmingly large, and an $\sim$ 0.1 dex systematic offset in [Fe/H] is not uncommon among different spectroscopic analyses (e.g., Torres et al. 2012). A similar offset was also found from a comparison with spectroscopic metallicities in Casagrande et al. (2010, see Table 5): Although there are only 11 stars available in the comparison, the mean difference is Δ[Fe/H] = 0.14 dex in the sense that SMT3 predicts higher metallicities. Given the systematic nature of the difference, we decided to adjust SMT3 metallicities for our sample stars by a constant offset (Δ[Fe/H] = 0.07 dex), to be consistent with the metallicity scale of VF05 (and MOOG).

The 8$^{\rm th}$ column in Table 6 ("[Fe/H]$_{\rm corr}$") lists metallicities from SMT3 after the above zero-point correction. In Figure 7 a black histogram shows a distribution of effective temperature (left panel) and that of metallicity (right panel) for all of our sample stars as obtained from SMT3. The red shaded histogram represents a subset of these stars, which was analyzed using MOOG. Our sample covers $4800 \lesssim T_{\rm eff}({\rm K}) \lesssim 5900$ and $-0.8 \lesssim$ [Fe/H] $\lesssim 0.2$, and there is no correlation found between $T_{\rm eff}$ and [Fe/H] in each of these two parallel approaches.

4. RESULTS

The goal of this work is to identify hypothesized subluminous field stars in the solar neighborhood, which have similar photometric properties with those in the Pleiades. Such stars are sub-luminous in the sense that they would reveal themselves as having fainter absolute magnitudes from *Hipparcos* than those inferred from MS fitting. If the *Hipparcos* parallaxes are correct, luminosities of these stars were overestimated in MS fitting for still unknown reasons. Since the luminosity of MS stars is strongly dependent on metallicity, below we first establish a metallicity sensitivity of stellar colors and magnitudes using previous star samples in the literature with accurate parallaxes and metallicities (§ 4.1). The comparison in M_V between *Hipparcos* and MS fitting is presented in § 4.2 for our KPNO sample. We utilize our metallicity measurements from both MOOG and SMT analyses to check our results against potential systematic errors in the adopted metallicity values. Although our sample selection was not designed to find young stars in the solar neighborhood, there are a small number of stars found in our sample with strong lithium absorptions and/or chromospheric activity levels that are characteristic of stars in the Pleiades. In § 4.3 we use these stars to test a hypothesis that the Pleiades' distance is over-estimated in MS fitting due to young ages of its members. Finally, we present our best estimate of a MS-fitting distance to the Pleiades based on the observed MS of the Hyades and empirical metallicity sensitivities of stellar colors and magnitudes (§ 4.4).

4.1. *Metallicity Sensitivity Function*

An absolute magnitude of an i^{th} star in our sample can be computed either based on the *Hipparcos* parallax ($M_{V,i}^{\rm HIP}$) or MS fitting ($M_{V,i}^{\rm MS}$). The difference between the two M_V estimates is equal to a difference in distance modulus:

$$\Delta M_{V,i} \equiv M_{V,i}^{\rm HIP} - M_{V,i}^{\rm MS} \quad (1)$$

$$= (V - M_V)_{0,i}^{\rm MS} - (V - M_V)_{0,i}^{\rm HIP}. \quad (2)$$

While $M_{V,i}^{\rm HIP}$ can be directly estimated from a V-band magnitude and a trigonometric parallax for individual stars, MS-fitting approach requires a well-defined set of color-magnitude relations over a wide range of metallicity. More specifically, $M_{V,i}^{\rm MS}$ in the above equations is a function of both temperature (or color) and metallicity, and should be known a priori to derive a distance from MS fitting. Within the temperature range of our sample, metal-poor MS stars are fainter than metal-rich stars at a given $B-V$ color, and the amount of offset in M_V as a function of metallicity can be constrained either from observations or from theory.

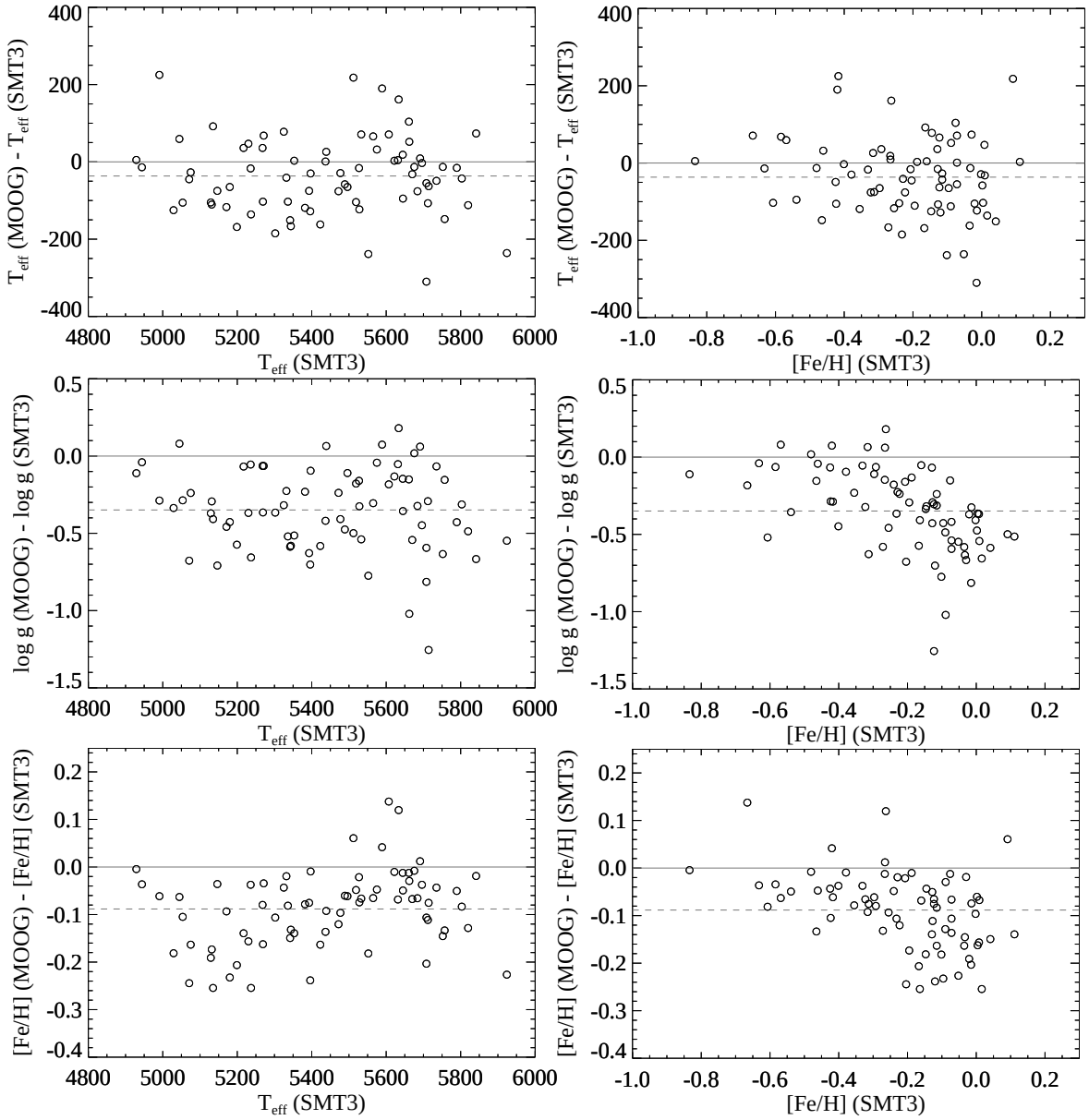

FIG. 4.— Comparisons of spectroscopic parameters between MOOG and SMT with the full three-parameter fitting (SMT3). The dashed line indicates a mean difference, while the solid line is a zero difference. In the bottom panels, metallicities from SMT3 represent raw values, while MOOG estimates are those with a zero-point adjustment (see text).

In this paper, we employed a purely empirical approach, instead of relying on theoretical stellar isochrones, to search for anomalously sub-luminous stars in the solar neighborhood. We utilized an observed MS of the Hyades at its well-known metallicity and distance (Pinsonneault et al. 2004), and applied metallicity effects on stellar colors and magnitudes. This was done by rewriting an absolute magnitude of a star as

$$M_{V,i}^{\rm MS} = M_V^{\rm Hyades}(X_i) + \overline{\delta M_V}([{\rm Fe/H}]_i), \quad (3)$$

where $M_V^{\rm Hyades}(X_i)$ is a M_V of the Hyades' MS at a given color (or temperature) of a star in X passband such as in $B-V$. The $\overline{\delta M_V}([{\rm Fe/H}]_i)$ represents a metallicity term, which may also depend on colors. However, the color range of our KPNO sample is sufficiently narrow that color-magnitude relations at different metallicities are almost parallel to each other (see theoretical lines in the top left-hand panel of Figure 1)[15], and $\overline{\delta M_V}$ can essentially be treated as a function of metallicity alone. Theoretical predictions can be used to derive a metallicity term in broadband colors, but they are still uncertain because of large remaining uncertainties in input physics and stellar model parameters, and ultimately need to be constrained against a well-defined set of observational data (e.g., An et al. 2007a,b, 2015). Comparisons of our sample stars with theoretical models will be discussed in the next paper of this series.

To derive a metallicity correction term in Equation 3 on an empirical basis, we employed the *Hipparcos* data themselves.

[15] The approximate behavior of stars with differing metallicities can be understood with a simply homology relation (e.g., Portinari et al. 2010, see their equation 4). Note, however, that the influence of helium enrichment should be disentangled in order to measure the metallicity effect on stellar luminosity.

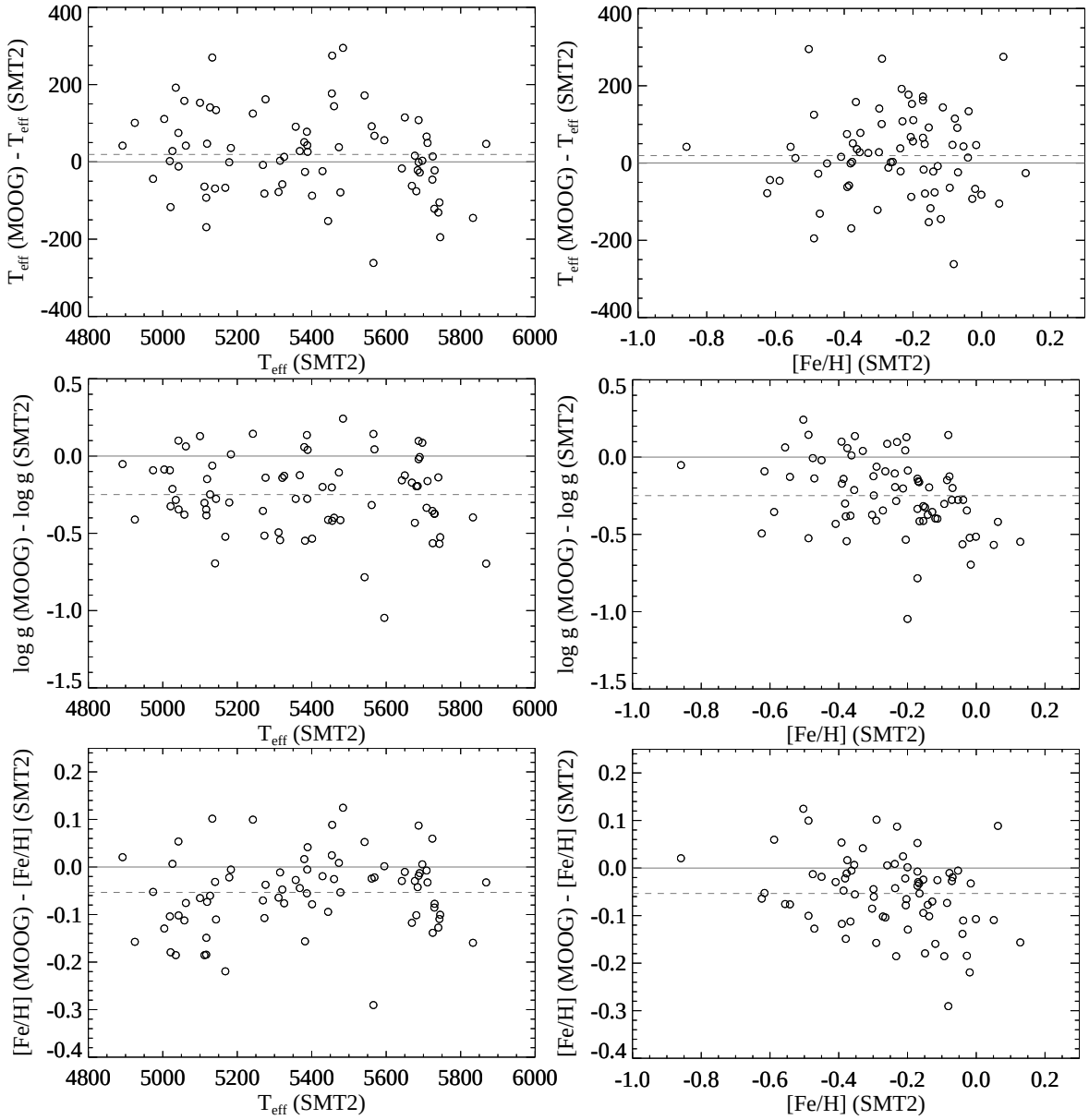

FIG. 5.— Same as in Figure 4, but comparisons with SMT analysis based on IRFM temperatures (SMT2).

Here, our core assumption in this paper is that parallaxes for the majority of stars in the *Hipparcos* catalog are correct, but only a small fraction of these stars, such as those in the Pleiades, have larger parallax errors than those specified in the catalog. For this, we computed a difference between M_V from *Hipparcos* and M_V from the Hyades' MS at a given color of a star:

$$\delta M_{V,i} \equiv M_{V,i}^{\rm HIP} - M_V^{\rm Hyades}(X_i) \quad (4)$$

$$= V_i + 5\log\pi_i + 5 - M_V^{\rm Hyades}(X_i), \quad (5)$$

where V_i and π_i are an observed V magnitude and a star's parallax, respectively. The average δM_V for a sufficiently large number of stars in a narrow bin of metallicity is

$$\overline{\delta M_V}([{\rm Fe/H}]) = \langle M_V^{\rm HIP}\rangle - M_V^{\rm Hyades}, \quad (6)$$

and yields an empirical correction to be added to the $M_V^{\rm Hyades}$ of a star (Equation 3). The $\overline{\delta M_V}$ can be computed for various bins in [Fe/H], and these corrections can be expressed as a metallicity sensitivity function in a given color index.

Using Equations 3 and 4, the difference between the MS-fitting and *Hipparcos*-based distance in Equation 1 can be expressed as

$$\Delta M_{V,i} \equiv M_{V,i}^{\rm HIP} - M_V^{\rm Hyades}(X_i) - \overline{\delta M_V}([{\rm Fe/H}]_i) \quad (7)$$

$$= \delta M_{V,i} - \overline{\delta M_V}([{\rm Fe/H}]_i). \quad (8)$$

Since the metallicity correction term $\overline{\delta M_V}([{\rm Fe/H}])$ depends only on metallicity, searching for anomalously sub-luminous stars with large differences in M_V between the MS-fitting and the *Hipparcos* distance is equivalent to finding outliers in δM_V at a given metallicity.

We utilized stars in VF05 with good parallaxes ($\sigma_\pi/\pi \leq 0.03$) to derive an empirical metallicity sensitivity function, or the amount of offset in M_V as a function of metallicity, in broadband colors. We restricted the sample to $0.7 \leq B -$

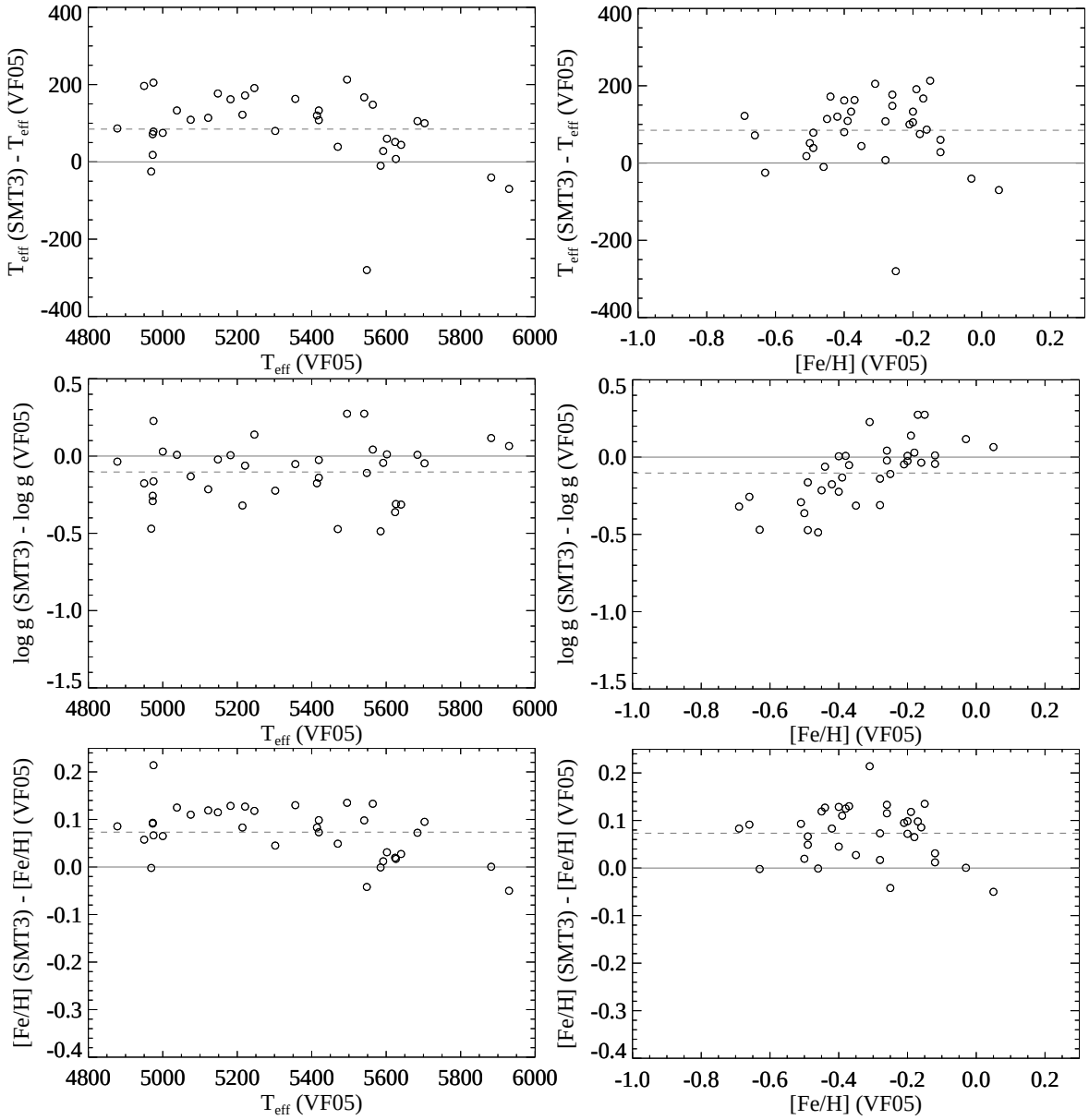

FIG. 6.— Same as in Figure 4, but showing comparisons between SMT3 and VF05. In the bottom panels, metallicities from SMT3 represent raw estimates, before applying a zero-point adjustment (see text).

$V \leq 1.0$ to make the sensitivity measurement suitable for our KPNO targets. The (conservative) lower limit ($B-V = 0.7$) was set to eliminate potential contaminations by bright turn-off stars. The top panel in Figure 8 shows δM_V of these stars computed using Equation 5 in $B-V$ colors. These values decrease towards higher metallicity, because metal-rich MS stars are brighter than metal-poor stars at a given $B-V$ color. The observed trend in this panel reflects the metallicity sensitivity function (Equation 6).

The observed metallicity sensitivity seen in the top panel of Figure 8 tends to become steeper at higher metallicities. On the other hand, our sample is restricted to those having metallicities below solar, where the observed trend can be approximated by a straight line. Another consideration when deriving a metallicity sensitivity function is that M_V estimated using Hyades' MS ($M_V^{\rm Hyades}$) must be equal to M_V from *Hipparcos* ($M_V^{\rm HIP}$) at the metallicity of the Hyades ([Fe/H] = +0.13), or $\delta M_V = 0$, by definition. However, there are more stars found with negative δM_V than those with positive values at [Fe/H]$\sim$ +0.13. This could be due to a scale error in metallicity or the presence of unresolved binaries in the sample, which are brighter than single MS stars, and therefore having systematically smaller δM_V. Without having a complete census on binarity, we simply proceeded with fitting a straight line to the data for stars with $-1.0 \leq$ [Fe/H] ≤ -0.1, as shown by the red line, forced to pass through our adopted reference point, the Hyades (cross mark). Our metallicity sensitivity line has a slope of -0.8 mag dex^{-1}, and is used in the following analysis as a reference value for the mean metallicity sensitivity function in $B-V$.

We additionally used stars in Casagrande et al. (2010) to independently check the above metallicity sensitivity function. We cross-identified stars in Casagrande et al. with the *Hipparcos* catalog using a $10''$ search radius along with stellar colors and magnitudes. In the bottom panel of Figure 8, stars

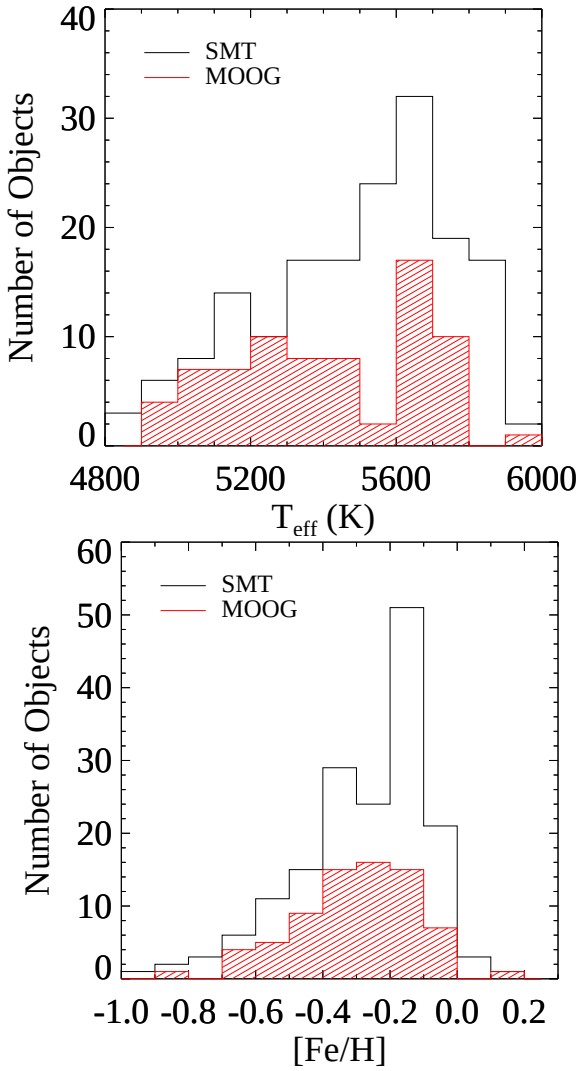

FIG. 7.— Distributions of effective temperature (left) and metallicity (right) of the KPNO samples as obtained using SMT3 (black histogram) and those from MOOG (red shaded histogram). Metallicities are those after applying a zero-point adjustment.

with fractional errors in parallax of better than 3% are shown in diamond and those with $\leq 7\%$ in circled points, with spectroscopic metallicities as reported in Casagrande et al. (2010). As in the top panel, we selected stars in $0.7 \leq B-V \leq 1.0$. The blue dashed line is a linear fit to stars in Casagrande et al. with $\leq 3\%$ fractional errors in parallax (red diamond points), and shows nearly the same slope as the one obtained using stars in VF05 (red solid line).

In Figure 8, the dispersion of the data points around the mean line is $\sigma(\delta M_V) = 0.12$ mag for VF05 and 0.10 mag for Casagrande et al. (2010), when only stars with good parallaxes ($\sigma_\pi/\pi \leq 0.03$) are used. Photometric errors in $B-V$ of ~ 0.02 mag, which is reasonable to assume, are translated into 0.1 mag error in M_V, because the slope of MS is about 5 on a $B-V$ CMD. The error in the observed V magnitude directly affects the error in δM_V (see Equation 5), but is negligible compared to that from a color error. A parallax error likely produces an error in δM_V of ~ 0.05 mag, and the error in [Fe/H] of ~ 0.05 dex is translated into 0.04 mag error in δM_V. All together, the error in δM_V is largely dominated by photometric color errors. The remaining errors could come from unresolved companions of binaries and/or an older age of a star than the Hyades (550 Myr), which would make stars look brighter than a single-star zero-age MS.

While the observed dispersion is close to our expectation, there are a few outliers in Figure 8 that are far below the metallicity sensitivity line, with the largest magnitude offset ΔM_V of about 0.5 mag. According to Equation 8, this offset corresponds to a larger *Hipparcos*-based absolute magnitude than M_V from MS fitting. A possibility is that $B-V$ color of a star is too blue by 0.1 mag, or that V mag is too large by 0.5 mag, but the sizes of photometric errors required are uncomfortably large. The other possibility is that a star's spectroscopic metallicity was overestimated by Δ[Fe/H] = 0.5, but again the expected error seems too large for a high-resolution spectroscopic analysis. In addition, this can be due to an overestimated parallax measurement in the *Hipparcos* catalog, which may pose a similar problem with the Pleiades stars. However, a parallax error cannot be condemned for a large ΔM_V unless other sources of errors are well understood. In the following analysis, we used our homogeneous KPNO data set with well-determined spectroscopic metallicities to better identify and characterize the properties of outliers in the δM_V versus [Fe/H] diagram.

4.2. *Magnitude Excess of KPNO Sample*

Figure 9 shows the same δM_V versus [Fe/H] plot as in Figure 8, but for our KPNO sample, where δM_V of stars and their errors are those listed in the second and third columns in Table 7. Stars with MOOG and SMT3 metallicities (both scaled to match the VF05 metallicities) are used in the top and the bottom panel, respectively. In each panel, the cross mark indicates the Hyades at the cluster's distance from *Hipparcos* ($\Delta M_V = \delta M_V = 0$), and the same red line as in the top panel of Figure 8 is shown for the empirical metallicity sensitivity function in $B-V$ CMDs. A magnitude excess in this study is defined as having a shorter *Hipparcos* distance than that from MS fitting, or a positive offset of a star from the mean metallicity function ($\Delta M_V > 0$). While our sample does not include stars in the Pleiades, we mark the position of the Pleiades as a blue diamond point at its well-known metallicity [Fe/H] = +0.04 (see references in An et al. 2007b). We found $\delta M_V = 0.40$ from 33 single MS stars in the Pleiades using the Hyades' MS. The *Hipparcos* distance of the Pleiades is shorter than the MS-fitting distance by $\Delta(m-M)_0 = \Delta M_V = 0.33$ (Pinsonneault et al. 1998; An et al. 2007b). Below we use $\Delta M_V = 0.33$ as a reference to judge whether stars in our KPNO sample are anomalously faint, or have a large magnitude excess, like those in the Pleiades at its *Hipparcos* distance.

In the top panel of Figure 9, a total of 74 field stars with MOOG metallicities are shown, representing the entire KPNO sample with parallax errors of better than 3%. In the bottom panel, 167 sample stars with SMT3 metallicities are shown with parallax errors of better than 7%. The red diamond points are a subset of these stars, having more accurate parallaxes ($\sigma_\pi/\pi \leq 0.03$). The vertical error bars are a quadrature sum of errors from photometry and parallax (see Equation 5). As in Figure 8, we included an error in δM_V from a photometric color, by multiplying a $B-V$ error by a slope of the Hyades' MS. In the bottom panel, horizontal error bars are metallicity errors reported by SMT; HIP 95727 is not displayed because of its large metallicity error (0.51 dex).

In Figure 9 the gray shaded region represents a forbidden area that was excluded from our color-magnitude selection of

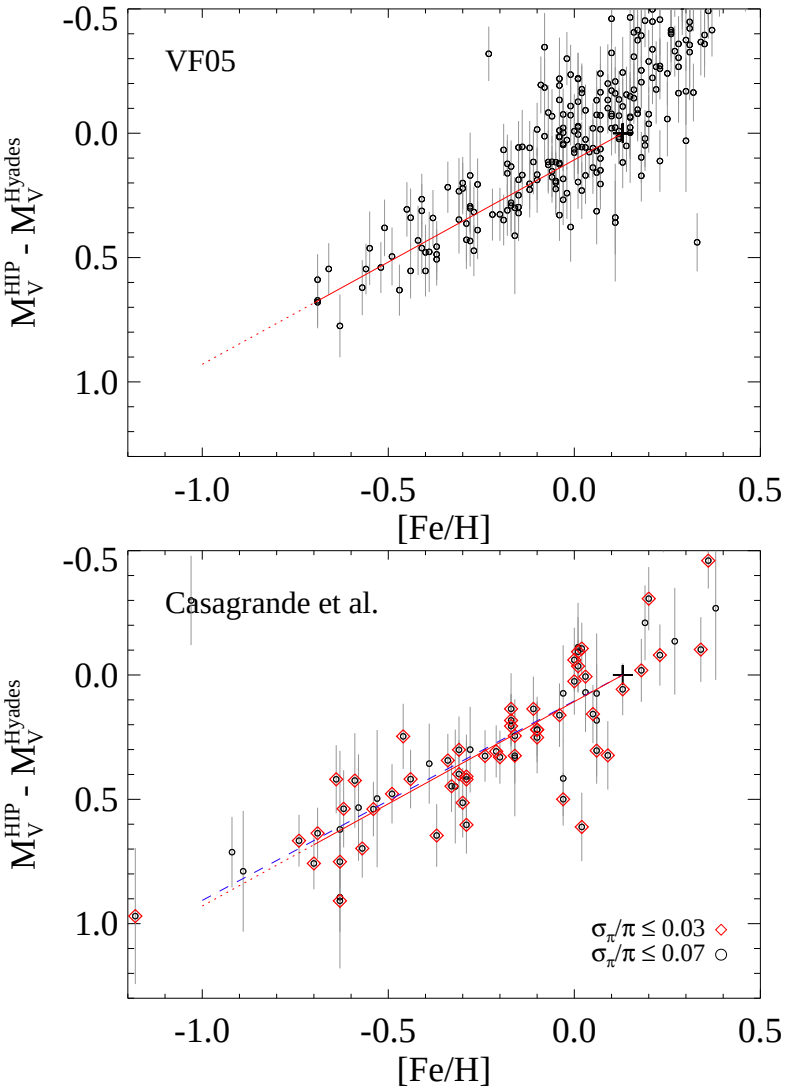

FIG. 8.— *Top:* The δM_V of the *Hipparcos* field dwarfs with metallicities from VF05. Only those in $0.7 \leq B-V \leq 1.0$ with good parallaxes ($\sigma_\pi/\pi \leq 0.03$) are shown. The red solid line is a linear fit to stars in $-0.7 \leq$ [Fe/H] ≤ -0.1, forced to match the position of the Hyades at [Fe/H] = +0.13 with a zero magnitude difference (black cross), and is shown in both panels. *Bottom:* Same as in the top panel, but showing calibration stars in Casagrande et al. (2010). The blue dashed line is a linear fit to stars with fractional errors in parallax of better than 3% (red diamond points), which passes through the black cross.

the KPNO sample. As shown in Figure 1, the upper limit in stellar brightness (or a lower limit in M_V) in our sample selection was set almost parallel to the MS of the Hyades, and any stars having $\delta M_V \lesssim 0.25$ mag were not included in our observing runs. The boundary of the shaded region is not a clear cut division, because the slope of the Hyades' MS is not exactly parallel to our color-magnitude selection. Nevertheless, our search for sub-luminous MS stars is almost unaffected by this sample bias since such stars would reveal themselves as having significantly faint M_V with the *Hipparcos* parallax, or a large ΔM_V at a given metallicity. On the other hand, a metallicity sensitivity function cannot be constructed using our field star sample alone because of a sample bias against intrinsically bright, metal-rich stars.

Considering the above sample bias, most of our KPNO stars in Figure 9 are distributed in the same manner as in Figure 8 and follow the empirical metallicity sensitivity function (red solid line). In the bottom panel, a distribution of the sample with $\leq 3\%$ parallax errors is tighter than that from the entire KPNO sample. A true dispersion of a magnitude excess from the mean sensitivity line [$\sigma(\Delta M_V)$] is difficult to measure for our sample due to the limit set by our sample selection (grey region). Nevertheless, metal-poor stars ($-0.7 \leq$ [Fe/H] ≤ -0.4) are relatively free from the sample bias, from which we found $\sigma(\Delta M_V) = 0.11$ mag for a rms dispersion of these stars with highly accurate parallaxes ($\sigma_\pi/\pi \leq 0.03$). On the other hand, the expected size of error in ΔM_V for individual stars is 0.16 mag from 2% errors in the photometry, $\sim 2\%$ error in parallax, and 0.067 dex error in metallicity (see above), which approximately matches the measured dispersion.

Figure 10 shows the same δM_V versus [Fe/H] diagrams as in the bottom panel of Figure 9, but in three different color bins: $0.6 \leq B-V < 0.7$ (top), $0.7 \leq B-V < 0.8$ (middle), and $0.8 \leq B-V \leq 1.0$ (bottom). The minimum δM_V of stars in $0.8 \leq B-V \leq 1.0$ is slightly larger than those for bluer stars. As described in § 2.1, this is because our color-magnitude selection, which was made using the Pleiades' MS, is not exactly parallel to the Hyades' MS (see the top left-hand panel in Figure 1). The Pleiades members progressively become

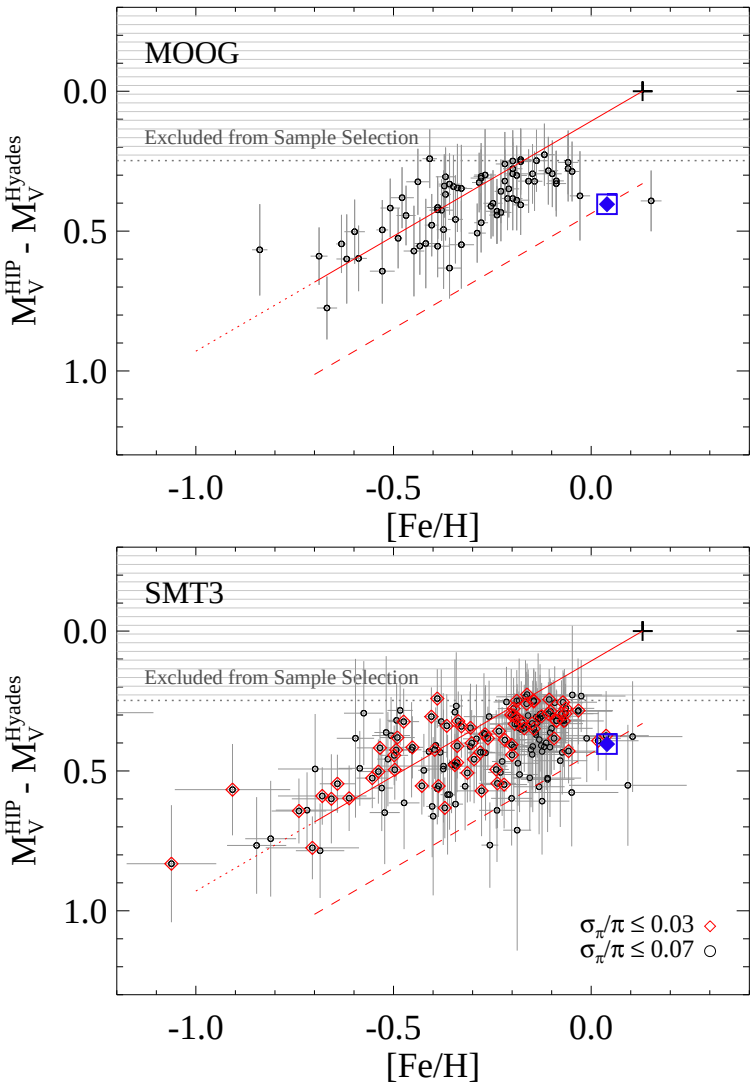

FIG. 9.— The δM_V of the KPNO sample with MOOG (top) and SMT3 (bottom) metallicity estimates. Stars in the top panel are those having good parallax measurements ($\sigma_\pi/\pi \leq 0.03$). The same set of stars are also shown as red diamond points in the bottom panel. The red solid line represents a mean metallicity sensitivity function as derived from the VF05 stars in the top panel of Figure 8. The blue diamond point with a box indicates the Pleiades, and its magnitude excess (ΔM_V) is shown by a red dashed line. The grey shaded area represents a δM_V limit set by our sample selection.

fainter than older stars with the same metallicity or those predicted from standard stellar models, most likely due to stellar activities. The effect is mild at $0.9 \lesssim B-V \lesssim 1.0$, but is not convincingly observed for stars with $B-V < 0.9$ (see Figure 20 in An et al. 2007b). We limited our sample to $B-V \leq 1$ since such activity-related change of stellar colors and magnitudes becomes severe for redder stars (Stauffer et al. 2003; An et al. 2007b). Other than a slight difference in the minimum δM_V, our sample stars in Figure 10 behave almost independently of color ranges.

While most of the KPNO sample stars have *Hipparcos* parallaxes that are consistent with MS-fitting distances, there are a few stars that have shorter *Hipparcos* distances. In the top panel of Figure 9, there is one such star found from the MOOG analysis (HIP 99965). In the bottom panel, which shows the same δM_V with SMT3 metallicities, none of the stars with accurate parallaxes ($\sigma_\pi/\pi \leq 0.03$; red diamond) has a larger magnitude excess than the Pleiades ($\Delta M_V = 0.33$; red dashed line). For the extended sample with $\sigma_\pi/\pi \leq 0.07$, a total of 9 stars exhibit larger ΔM_V than the Pleiades, which account for $\sim 5\%$ of the entire KPNO sample. These are HIP 5313, HIP 10276, HIP 73138, HIP 73845, HIP 74126, HIP 75446, HIP 78336, HIP 81831, and HIP 97668. The ΔM_V estimates of our sample stars, including those with the largest magnitude excess, are listed in the 4th and 5th columns in Table 7. The errors in ΔM_V are larger than those of δM_V due to an additional contribution from spectroscopic metallicity errors. Figure 11 shows ΔM_V of stars as a function of the SMT3 metallicity. The symbols are the same as in the bottom panel of Figure 9. The statistical significance of the above 9 stars is less ($\sim 2\sigma$) than that of the Pleiades, since individual stars have larger errors in δM_V from photometry, metallicity, and parallax than in the case of a cluster where a large number of stars can be used together to increase an internal precision of the measurements.

Because stars with large ΔM_V are all having relatively large parallax errors, it is unclear whether the large magnitude excess was induced by random parallax measurement errors, or by a hidden systematic error in the *Hipparcos* parallax, which was originally suggested by Pinsonneault et al. (1998) to explain the short Pleiades distance. We also analyzed spectra

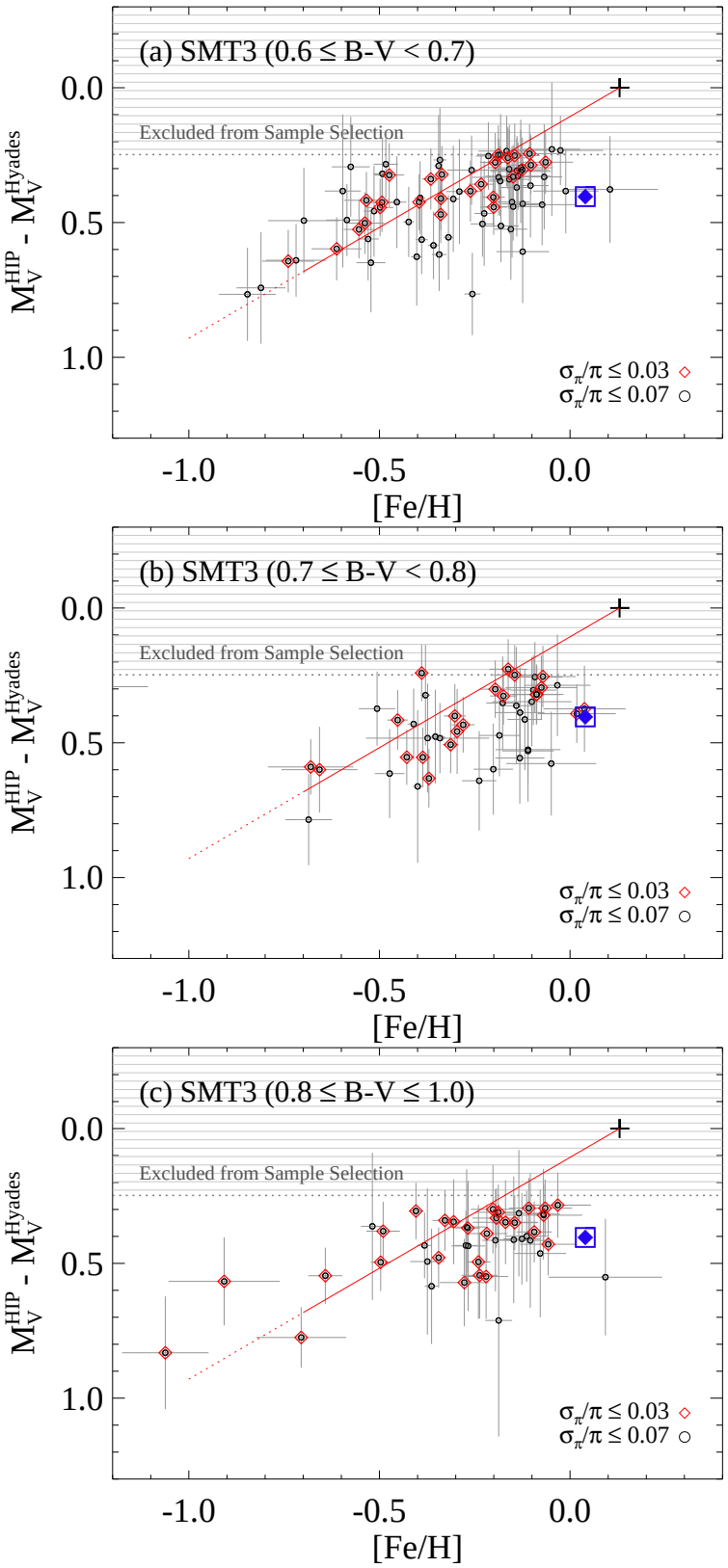

FIG. 10.— Same as in the bottom panel of Figure 9, but displaying KPNO samples in different color ranges: (a) $0.6 \leq B-V < 0.7$, (b) $0.7 \leq B-V < 0.8$, and (c) $0.8 \leq B-V \leq 1.0$.

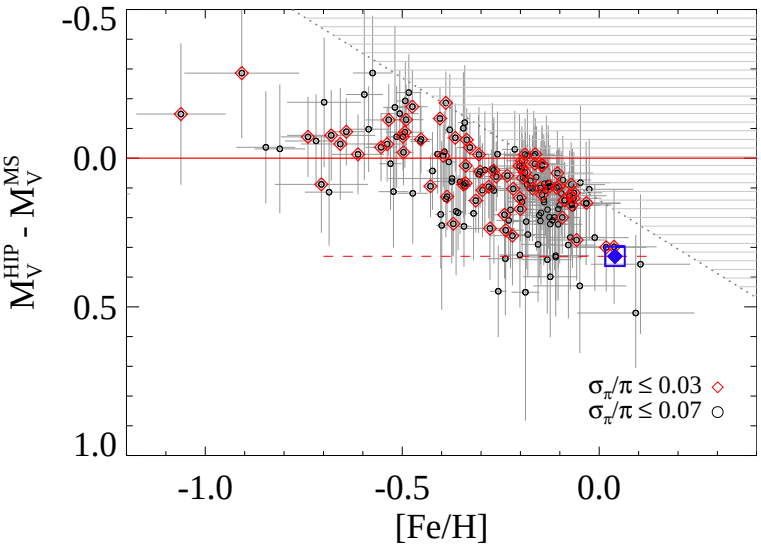

FIG. 11.— Same as in the bottom panel of Figure 9, but displaying ΔM_V or a difference between a MS-fitting distance modulus and that from the *Hipparcos* parallax.

of the above 9 stars with the largest magnitude excess using MOOG (Table 2), which have not been originally included in our MOOG analysis due to their large parallax errors. With MOOG metallicities, six out of the 9 stars were still having larger ΔM_V than the Pleiades. Their ΔM_V estimates are shown in the 6th and 7th columns in Table 7, along with those for all stars analyzed using MOOG.

In addition to $B-V$ colors, we repeated the above experiment with $V-K_s$ colors using the MS of the Hyades in the $V-K_s$ versus V CMD to compute δM_V of individual stars. These δM_V estimates are listed in the 8th and 9th columns in Table 7, which are not equal to δM_V from $B-V$ because of a different color-$T_{\rm eff}$ relation in $V-K_s$. The $V-K_s$ is also less sensitive to metallicity than $B-V$, while being more sensitive to unresolved binaries, giving an independent look at the distribution of stars in the δM_V versus [Fe/H] diagram. In addition, photometry from a uniform all sky survey like 2MASS can provide more reliable estimates in δM_V.

As in $B-V$, we derived a mean empirical metallicity sensitivity in $V-K_s$ using the same sample stars in VF05 with good parallaxes ($\sigma_\pi/\pi \leq 0.03$). The result is shown in the top panel of Figure 12, where we used and displayed only those in $1.6 \leq V-K_s \leq 3.0$ to avoid a contamination by turnoff stars. Stars with $-1.0 \leq$ [Fe/H] ≤ -0.1 and $\delta M_V \geq -0.5$ were used in the linear regression for the metallicity sensitivity function in $V-K_s$ (red solid line). The slope of this line is –0.28 mag dex^{-1}, which is significantly shallower than that from $B-V$ (Figure 8). The lower panel in Figure 12 additionally shows a metallicity sensitivity function in $V-K_s$ (blue line) as derived from an independent set of stars ($1.6 \leq V-K_s \leq 3.0$) in Casagrande et al. (2010) with good parallaxes ($\sigma_\pi/\pi \leq 0.03$), of which slope (–0.25 mag dex^{-1}) is almost identical to the one from the top panel (red line).

Our KPNO sample stars are shown in Figure 13 where δM_V was derived from $V-K_s$ CMDs. As in Figure 9, MOOG metallicities are used in the top panel, and [Fe/H] from SMT3 are used in the bottom panel. Stars with highly accurate parallaxes ($\sigma_\pi/\pi \leq 0.03$) are shown in the top panel and indicated by red diamond points in the bottom panel. The red solid line is the mean metallicity sensitivity function from the top panel in Figure 12. Most of our sample stars follow this trend, if one takes into account the fact that our sample selection was biased against stars with small (negative) δM_V. The δM_V of the Pleiades, as determined from the Hyades' MS, is $\delta M_V = 0.33$ (or $\Delta M_V = 0.30$), and is shown as a blue diamond symbol.

In total, 9 stars were identified as having larger ΔM_V than the Pleiades (red dashed line): HIP 5313, HIP 56092, HIP 71720, HIP 75446, HIP 77810, HIP 81831, HIP 97668, HIP 99965, and HIP 114385. However, only about half of them (HIP 5313, HIP 75446, HIP 81831, and HIP 97668) show as large ΔM_V as the Pleiades in $B-V$ (Table 7), suggesting that photometric errors would have made a significant contribution to an error in ΔM_V. We also analyzed these stars using MOOG (Table 2), since they were not originally included in our MOOG analysis (except HIP 99965) due to large parallax errors ($\sigma_\pi/\pi > 0.03$). Nevertheless, we found that the difference in metallicity between the two approaches is small. Its impact on ΔM_V is further reduced by the relatively weak metallicity dependence in $V-K_s$ (–0.28 mag dex^{-1}), resulting in a negligible difference in ΔM_V.

Figure 14 shows positions of the KPNO samples in equatorial coordinates, which is by design randomly distributed at $\delta > -30^\circ$ in our observing programs. The red bull's-eyes are the positions of the 9 stars with the largest magnitude excess in $B-V$ CMDs, and red triangles are those from $V-K_s$. In either of the cases, these stars are not spatially correlated with each other, nor do they show a spatial correlation with the location of the Pleiades (blue diamond point). Also, they are not associated with any of the fundamental great circles, such as the ecliptic (orange line) or the Galactic plane (blue line).

Our result shows that there are a small fraction of stars with sufficiently large ΔM_V, but their statistical significance is only marginal (a 2σ level). On the other hand, we failed to unambiguously identify stars with a large magnitude excess like the Pleiades, independently of a spectroscopic analysis technique and a color index employed, among those having good parallaxes ($\sigma_\pi/\pi < 0.03$). This may suggest that stars with the Pleiades-like phenomenon are rare, at least among nearby field stars with good parallax measurements. To confidently identify stars with (still unknown) systematic errors in parallax, it would be necessary to further shrink the size of errors in photometry and metallicity.

4.3. *Young Age and Stellar Activity*

Young stars often exhibit chromospheric activities with large stellar spots, which are thought to be related with their large angular momenta. All together, one can naively expect that either of these effects could somehow modify stellar energy distributions, making their observed broadband colors or magnitudes deviate from those of older stars. Such color anomalies have already been observed from late K-type dwarfs in the Pleiades (Stauffer et al. 2003), but our KPNO sample covers spectral types earlier than ∼K2, which helps to avoid issues on the potential modifications of colors and magnitudes by stellar activity and/or young age. Below we focus on young and/or active stars on the δM_V versus [Fe/H] diagram and see if these stars have systematically shorter *Hipparcos* distances than older stars. This will directly test a hypothesis that the longer Pleiades distance from MS fitting is due to yet unknown physics of young/active stars in the cluster (van Leeuwen 1999).

4.3.1. *Lithium Absorptions*

The color-magnitude selection of our sample is biased against the most metal-rich stars in the disk, and therefore probably does not favor a selection of young ($\lesssim$ 200 Myr) stars in the solar neighborhood. On the other hand, very young stars ($\lesssim$ 30 Myr) are also difficult to detect in our survey because low-mass pre-MS stars are brighter than MS at a given color. We measured EWs of lithium absorption at 6707.70 Å for our KPNO stars, and found that about 25% of the entire KPNO sample (N = 42) show an EW of Li larger than 5 mÅ. However, a majority of them show weak absorptions, suggesting that most of our sample stars including those with non-detections are relatively old. Among these, however, a small number of our KPNO spectra revealed a relatively strong Li absorption, implying young ages of these objects. The EWs of stars having W(Li) $>$ 5 mÅ are listed in the last column of Table 7.

While the Li line strength becomes weaker as a star gets older, an EW of lithium is also strongly dependent on stellar colors (or mass) by different depths of outer convective cells and by different amounts of angular momentum. This is shown in the top panel of Figure 15, which displays lithium EWs of MS

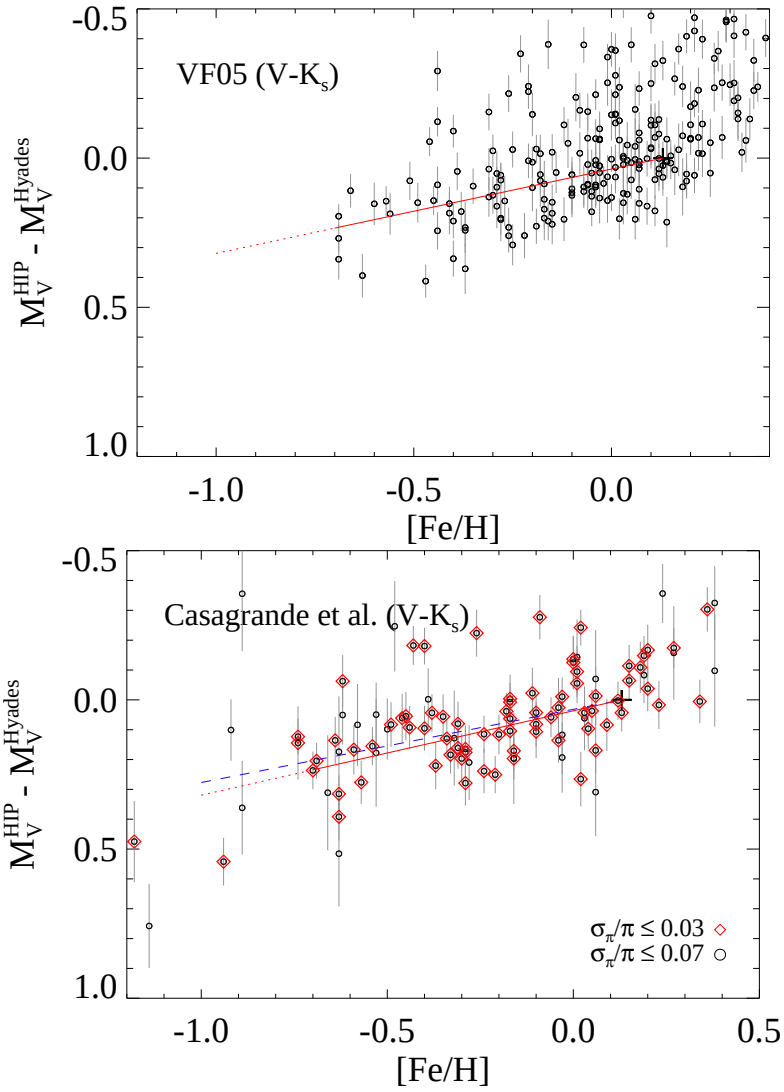

FIG. 12.— Same as in Figure 8, but in $V - K_s$ colors.

stars in three open clusters as a function $B - V$ (see Soderblom 2010): the Pleiades (blue open circle, Butler et al. 1987; Soderblom et al. 1993a; Garcia Lopez et al. 1994; Jones et al. 1996; Jeffries 1999), the Hyades (black open box, Soderblom et al. 1990, 1995; Thorburn et al. 1993), and M67 (open diamond, Hobbs & Pilachowski 1986; Spite et al. 1987; Garcia Lopez et al. 1988; Pasquini et al. 1997; Jones et al. 1999; Randich et al. 2002) at the age of 100 Myr, 550 Myr, and 4 Gyr, respectively. On top of these, our KPNO sample stars are marked by red closed circles. Only couples of stars in our sample fall into the range of Li EWs covered by the Pleiades members, which is not surprising given that our sample selection on a color-magnitude diagram was not designed to find youngest stars in the solar neighborhood. Due to a relatively small number of such stars, we selected young stars as those having larger Li EWs than those found in the Hyades as shown by a dashed line. This selection includes 9 stars (HIP 21276, HIP 60074, HIP 63322, HIP 72703, HIP 76674, HIP 77810, HIP 82388, HIP 108774, and HIP 114385). The one having an exceptionally large Li EW [W(Li) $\approx$ 120 mÅ] at $B - V$ = 0.87 is HIP 63322.

The bottom panel in Figure 15 shows the same δM_V versus [Fe/H] diagram of stars as in the bottom panel of Figure 9 with SMT3 metallicities, but displaying stars with a lithium EW larger than 5 mÅ. The red boxed points are young stars selected above as having largest Li EWs. As seen in this panel, a distribution of stars with lithium absorptions is not dissimilar to those seen from older stars (Figure 9). Among these, three stars (HIP 5313, HIP 74126, and HIP 78336) exhibit a larger magnitude excess than the Pleiades ($\Delta M \geq 0.33$), but they do not show a sufficiently strong Li absorption. More importantly, none of the above selected young stars exhibit larger ΔM_V than the Pleiades. Even if the sample is further restricted to five stars with W(Li) $>$ 100 mÅ, having almost identical properties to those in the Pleiades, their ΔM_V values show no systematic offset with respect to the empirical metallicity sensitivity function (red solid line). On the other hand, if the Pleiades' distance is short because of the young age of its stars, we would expect that stars having similar Li strength with the Pleiades members should have systematically large ΔM_V. Therefore, our result in Figure 15 suggests that the short Pleiades' distance cannot be condemned to somehow modified color-magnitude relations for young stars in the cluster, and that MS-fitting distances for young stars, with spectral types earlier than $\sim$K2, are sufficiently close to

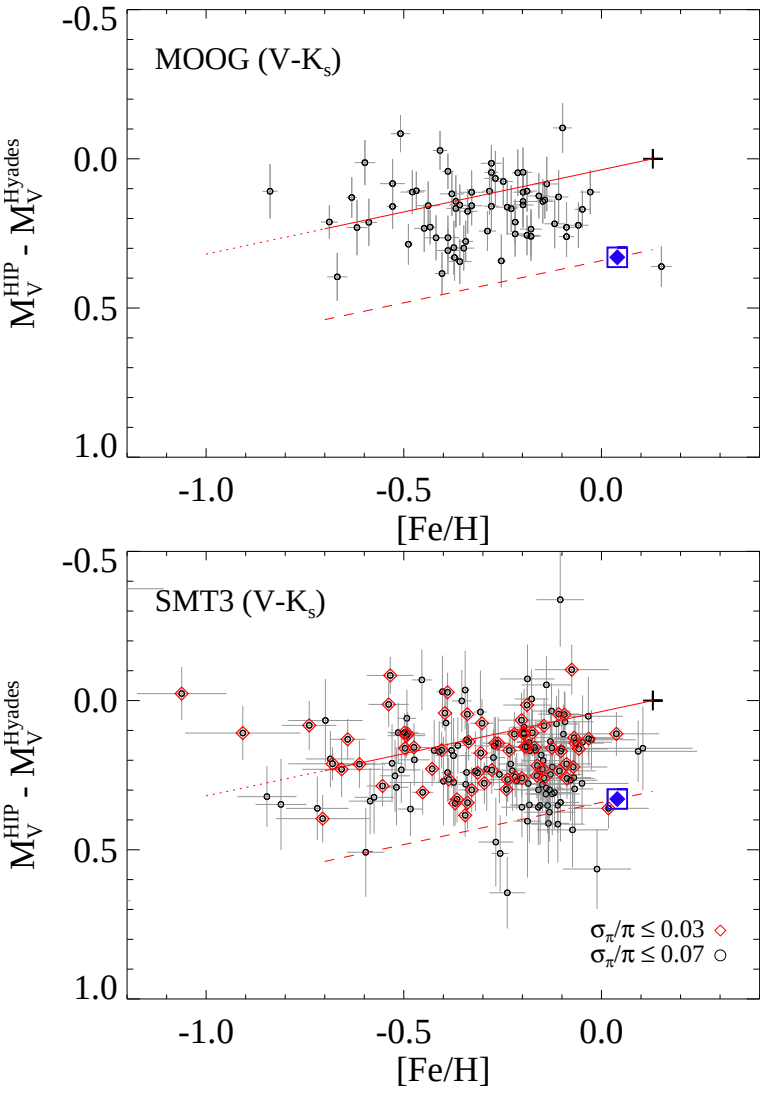

FIG. 13.— Same as in Figure 9, but in $V - K_s$ colors.

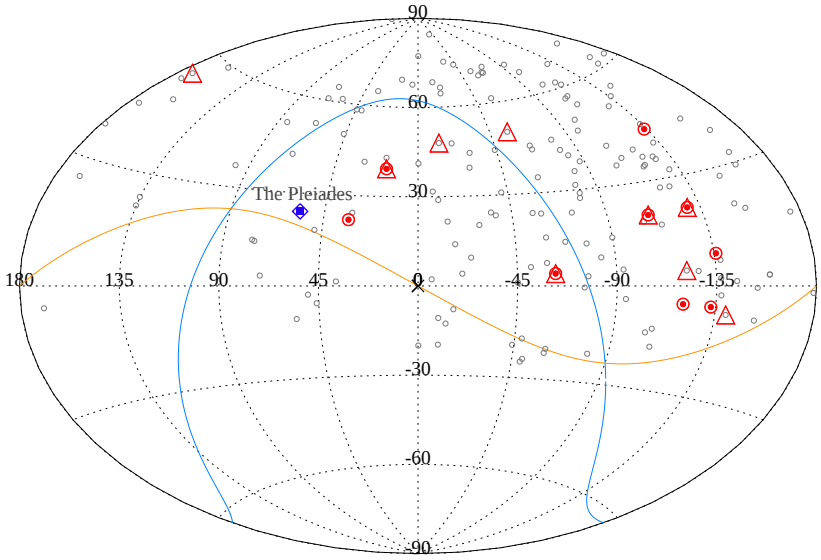

FIG. 14.— Distribution of the KPNO sample stars in equatorial coordinates. Stars with a larger magnitude excess than those of the Pleiades (blue diamond) in $B - V$ and $V - K_s$ CMDs are shown in red bull's-eyes and triangles, respectively. The ecliptic and the Galactic plane are shown in an orange and a blue line, respectively.

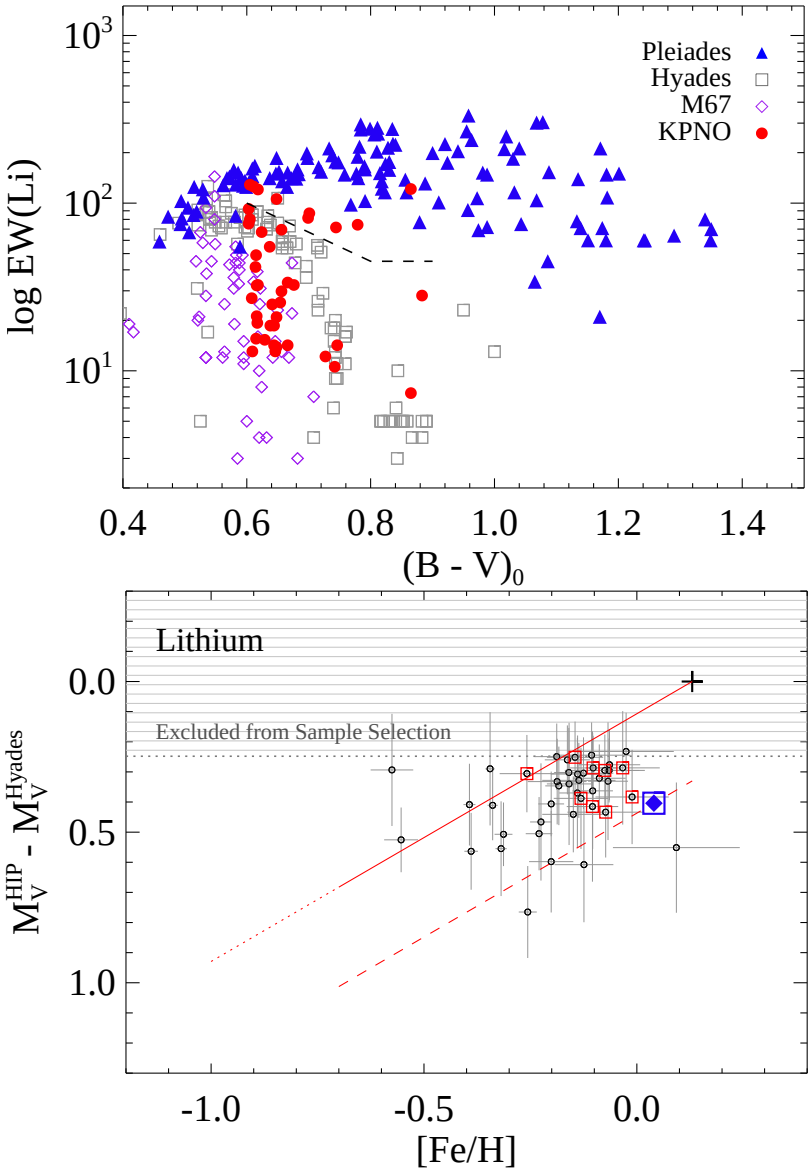

FIG. 15.— *Top:* EWs of lithium 6707 Å for the KPNO sample (red filled circles). EWs from open clusters are shown for the Pleiades (100 Myr; blue filled triangle), the Hyades (550 Myr; grey open box), and M67 (4 Gyr; open diamond). Our selection of young stars is indicated by a dashed line. *Bottom:* Same as in the bottom panel of Figure 9, but displaying stars with lithium 6707 Å absorptions ($\geq$ 5 mÅ). Stars with EWs larger than the dashed line in the top panel are shown in red squares.

those derived using color-magnitude relations for older stars.

Figure 16 shows CMDs of the Pleiades (Stauffer et al. 2007; Kamai et al. 2014) assuming the short (left panel) and the long (right panel) distance scale of the cluster, respectively. The most recent *Hipparcos* distance in van Leeuwen (2009) is used in the left panel. For the long distance scale, we used a weighted average distance $(m-M)_0 = 5.647 \pm 0.013$ (134.7 pc) from a number of geometric measurements (trigonometric parallaxes and binary solutions) listed in An et al. (2007b) and the VLBI measurement (Melis et al. 2014). We assumed $E(B-V) = 0.032$ for the Pleiades (An et al. 2007b) with color-dependent reddening and extinction laws (An et al. 2007a). The red open circles are our KPNO stars selected as having strong Li absorptions. For an apple-to-apple comparison with the Pleiades stars, we corrected their V-band magnitudes for a metallicity difference from the Pleiades ([Fe/H]= +0.04) using the empirical metallicity sensitivity function (i.e., red line in Figure 8). As these stars have lower metallicities than the Pleiades, they become brighter with these corrections.

The comparison with the Pleiades' CMDs in Figure 16 shows that Li-rich young stars are consistently brighter than the MS of the Pleiades by $\Delta M_V \approx 0.25$ when the *Hipparcos* distance is assumed (left-hand panel).[16] On the other hand, the long distance scale of the cluster leads to an excellent match of young field stars with the observed MS of the Pleiades. An absolute metallicity scale for our sample could be in error. However, $\Delta M_V = 0.08$ mag is expected if we have consistently overestimated our metallicities (or equivalently underestimated the Pleiades' metallicity) by Δ[Fe/H] = 0.1, which is far smaller than what is required to explain the $\Delta M_V \approx 0.25$ difference with the Pleiades' MS in the left panel.

In fact, most of these Li-rich stars are fainter than the mean MS relation at a given metallicity (with respect to the mean empirical metallicity sensitivity function) because of the sample selection bias as delineated by a shaded area in the bottom panel of Figure 15. Therefore, the red circles in Figure 16 represent approximately half of a Li-rich population in a given metallicity range, and constitute only a lower half of the brightness distribution. Nonetheless, missing Li-rich stars would be found above the red circles in the $B-V$ CMD (Figure 16), and would make the agreement with the Pleiades' MS even worse if the *Hipparcos* parallax is assumed for the cluster's distance. Figure 16 simply restates our conclusion that the Pleiades distance in van Leeuwen (2009) is too short and cannot be explained with the young age of cluster members.

4.3.2. *Stellar Activity Indices*

One of the most frequently used activity indicators is $R'_{\rm HK}$ index, which measures the chromospheric emission line strength of Ca II H and K at 3933.7 Å and 3968.5 Å in the central part of its broad absorption profile, normalized by photospheric continuum emissions (see Noyes et al. 1984). The $R'_{\rm HK}$ is a function of $T_{\rm eff}$ or colors, and is known to decrease with stellar ages (see Soderblom 2010). This is shown in the top panel of Figure 17, where $R'_{\rm HK}$ measurements from individual stars in three fiducial open clusters (Pleiades, the Hyades, and M67; Mamajek & Hillenbrand 2008) are displayed (see also Soderblom 2010). The $R'_{\rm HK}$ measurements from the Pleiades show a large scatter, indicating a star-to-star variation in chromospheric emissions, and a separation from those in the Hyades is not clearcut. Nevertheless, the cluster observations clearly suggest a systematic change of $R'_{\rm HK}$ with age.

In the top panel of Figure 17, our KPNO sample stars are indicated by red closed circles on top of the cluster observations. We took a large compilation of S-index measurements in the literature (Pace 2013, see references therein). In total, 93 stars in our sample have valid S-index measurements. Following Pace (2013), we took the average of a minimum and a maximum S-index values for each star, whenever there are repeat measurements, as a proxy for a time-averaged chromospheric activity level. We adopted a procedure in Noyes et al. (1984) to convert S index into $R'_{\rm HK}$.

Evidently, most stars in Figure 17 have similar $R'_{\rm HK}$ values with those in M67, suggesting old ages of these stars. On the other hand, there are approximately a dozen stars with $R'_{\rm HK}$ values that are comparable to those in the Pleiades. We took $\log R'_{\rm HK} = -4.5$ (dashed line) to select 11 likely young stars in our sample (HIP 4907, HIP 21276, HIP 60074, HIP 63322, HIP 63636, HIP 76674, HIP 77810, HIP 82388, HIP 106231, HIP 108774, and HIP 111888). Most of the Li-rich stars were also selected as having a strong chromospheric activity. Remaining Li-rich stars (HIP 72703 and HIP 114385) either do not have a $R'_{\rm HK}$ measurement in the literature or have a value near $\log R'_{\rm HK} = -4.5$. Nevertheless, our selection of active stars from $R'_{\rm HK}$ includes many Hyades dwarfs, and the separation of young stars from older populations is not as clear as in Figure 15 based on a lithium absorption.

The bottom panel of Figure 17 displays stars with $R'_{\rm HK}$ measurements on the δM_V versus [Fe/H] diagram with SMT3 metallicities. As expected, most of these stars are old, and are found along the mean metallicity sensitivity function (red solid line). Meanwhile, the boxed points are stars with $\log R'_{\rm HK} > -4.5$, and none of these chromospherically active stars show a larger magnitude excess than the Pleiades ($\Delta M_V > 0.33$). This result reiterates our conclusion above based on Li-rich stars that a young age of stars does not significantly modify color-magnitude relations for MS dwarfs.

In addition to $R'_{\rm HK}$ index, we collected X-ray luminosities of our sample stars from the NASA Exoplanet archive (Ramirez et al. 2013), and looked into the properties of stars selected based on X-ray luminosity. The X-ray luminosities show tight correlations with chromospheric activities such as $R'_{\rm HK}$ (Mamajek & Hillenbrand 2008), and can be used to trace young populations in the disk. However, measurements of X-ray luminosity are available only for 10 stars in our sample (Huensch et al. 1998; Hünsch et al. 1999; Schmitt & Liefke 2004). Among these, only two star (HIP 21276, HIP 106231) exhibit a higher X-ray luminosity than those in the Pleiades ($L_{\rm X} = 29.00$ ergs s^{-1}; Daniel et al. 2002). However, these stars have a significantly smaller magnitude excess than the Pleiades members. Although the number of stars with X-ray luminosities in the literature is small, it is clear that active stars in our sample have the same photometric properties as those for older stars. We conclude that stellar activity or young age of stars have a little impact (if any) on a large magnitude excess.

4.4. *Empirical MS-fitting Distance to the Pleiades*

Given the lack of evidence on anomalous color-magnitude relations for young/active stars with $0.6 \leq B-V \leq 1.0$, a

[16] This does not contradict with our sample selection (§ 2.1), in which we selected stars that are near or below the MS of the Pleiades assuming the van Leeuwen (2009) distance, because of the metallicity corrections as described above.

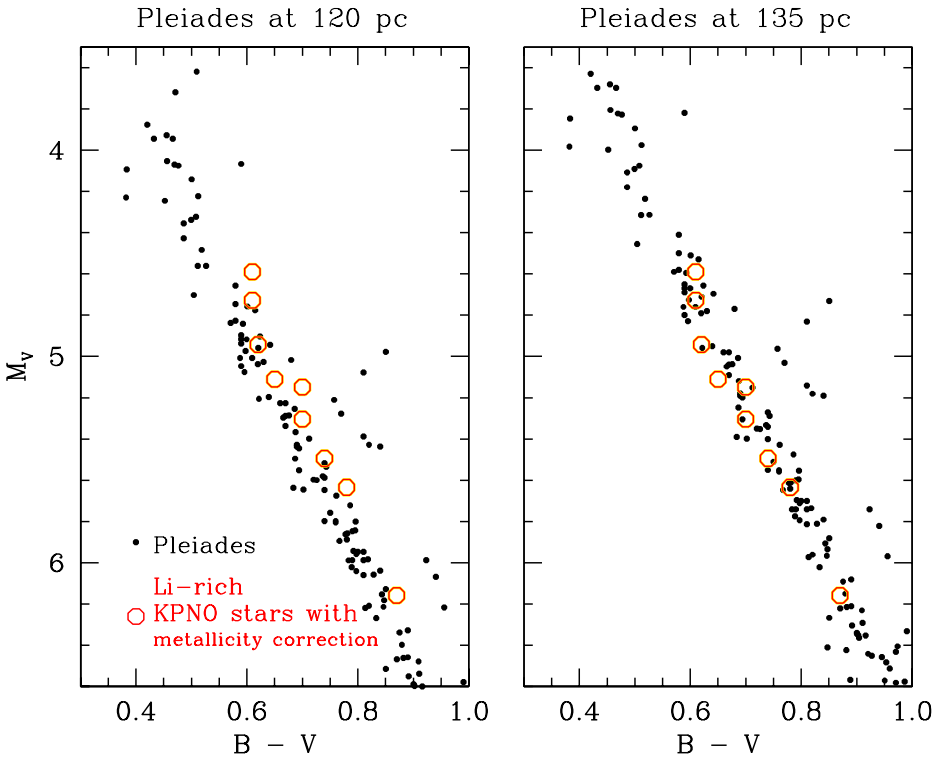

FIG. 16.— CMDs of the Pleiades (black points) assuming the *Hipparcos* parallax measurement in van Leeuwen (2009) (left panel) and the mean distance of the cluster from a number of geometric distance measurements except that from *Hipparcos* (right panel). The $E(B-V) = 0.032$ is assumed for hypothetical zero-color stars in the cluster with color-dependent reddening laws. The red open circles are Li-rich KPNO stars (those above the dashed line in Figure 15) with V-band magnitudes corrected for a metallicity difference from the Pleiades (see text).

purely empirical MS-fitting distance to the Pleiades can be obtained using the observed MS of the Hyades and the empirical metallicity sensitivity function as derived from the *Hipparcos* dwarfs. We assumed $E(B-V) = 0.032$ for the Pleiades (see above) and obtained $(m-M)_0 = 5.657 \pm 0.017$ and 5.669 ± 0.024 (statistical) in the $B-V$ and $V-K_s$ CMDs, respectively, using photometry of single MS stars of the cluster (An et al. 2007b) in $0.6 \leq B-V \leq 1.0$ and the corresponding range in $V-K_s$. We corrected distance moduli for a metallicity difference between the Pleiades and the Hyades, based on the empirical metallicity sensitivity functions in each of the color indices (red lines in Figure 8 and 12), which results in $(m-M)_0 = 5.585 \pm 0.023$ and 5.644 ± 0.025 in the $B-V$ and $V-K_s$ CMDs, respectively, where the errors are a quadrature sum of errors in fitting and metallicity ($\sigma_{[Fe/H]} = 0.02$). The average distance modulus of the Pleiades from the two CMDs becomes $(m-M)_0 = 5.615 \pm 0.030$; the error represents half of the difference in distance modulus. This purely empirical distance modulus is in perfect agreement with the mean geometric distance modulus of the cluster [$(m-M)_0 = 5.647 \pm 0.013$], but is significantly longer than the *Hipparcos*-based distance $(m-M)_0 = 5.40 \pm 0.03$ (van Leeuwen 2009).

5. SUMMARY

The debate on the Pleiades distance has continued even after the new reduction of the *Hipparcos* parallaxes (van Leeuwen 2009), which predicts ~ 0.3 mag fainter magnitudes of the cluster stars than those expected from MS fitting or other independent distance determinations. In this study, we tested a hypothesis that the long photometric distance of the Pleiades is due to anomalous colors or magnitudes of its cluster members, by searching for hypothesized sub-luminous field stars in the *Hipparcos* catalog. For comparison with the *Hipparcos* parallax, we derived accurate metallicities of 170 nearby G- and K-type field dwarfs based on high S/N ratios, high-resolution spectra, employing two independent spectral analysis techniques (MOOG and SMT). Our photometric distances based on these metallicities are purely empirical, being independent of any theoretical stellar isochrones, and relies on the observed MS of the Hyades and the metallicity dependence of colors, which was derived from the *Hipparcos* parallaxes and our metallicity measurements for a large number of field stars.

Among stars with highly accurate parallaxes ($\sigma_\pi/\pi \leq 0.03$), we could identify only one star from a $B-V$ CMD with a larger magnitude excess (ΔM_V) than the Pleiades, or a shorter *Hipparcos*-based distance by $\Delta(m-M)_0 = \Delta M_V \geq 0.33$, from the MOOG analysis. However, none of these stars in our sample have a larger magnitude excess than the Pleiades when the SMT metallicities are employed. For an extended sample with $\sigma_\pi/\pi \leq 0.07$, we identified 9 stars with $\Delta M_V \geq 0.33$, but the differences in distance modulus of these stars are only marginal. Furthermore, only six out of the 9 stars remain to show a large magnitude excess with an independent analysis technique from MOOG. In addition to $B-V$, we repeated the above exercise with $V-K_s$ colors, and found that only 3 stars identified as having $\Delta M_V \geq 0.33$ from $B-V$ have larger magnitude excesses than the Pleiades in $V-K_s$. Therefore, their oddity may not be surprising at all, and can be understood from errors in photometry, metallicity, and parallax.

Although we could not identify stars with large magnitude

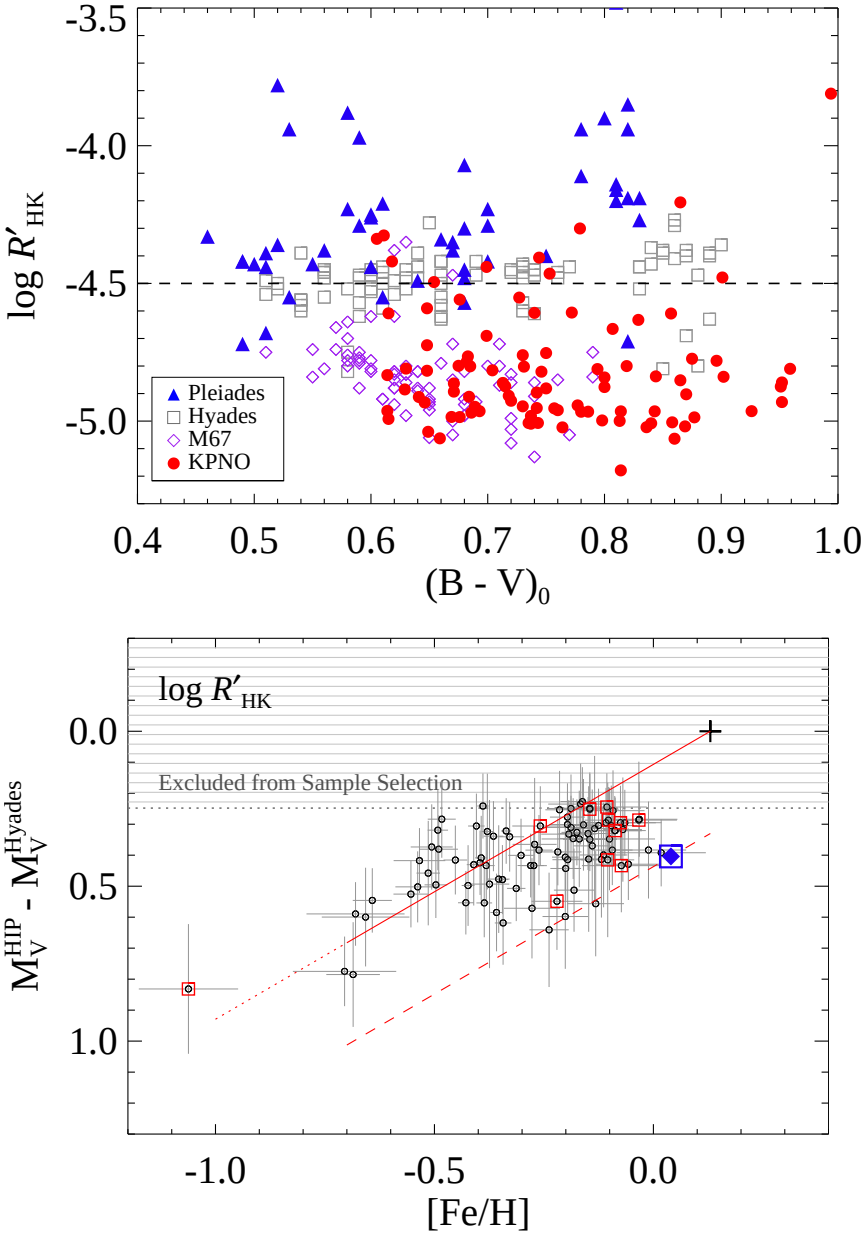

FIG. 17.— *Top:* R'_{HK} values for the KPNO sample in comparison with cluster measurements: the Pleiades (100 Myr; blue filled triangle), the Hyades (550 Myr; grey open box), and M67 (4 Gyr; open diamond). The black dashed line represents our division of active/inactive stars based on R'_{HK}. *Bottom:* Same as in the bottom panel of Figure 9, but displaying stars with R'_{HK} values available in the literature. The red boxed points are stars with $\log R'_{HK} > -4.5$.

excesses at a statistically significant level, we were able to reject a hypothesis that these outlying stars are mostly young or active stars. We selected young/active stars based on the Li 6707 Å absorption, R'_{HK}, or X-ray luminosity, and found that photometric distances of these young/active stars are not greatly different from the *Hipparcos* parallaxes. Although only a few stars in our sample may be as young as those in the Pleiades, none of these stars show larger differences in distance from *Hipparcos* than the Pleiades. While more young star samples can be used to better quantify the difference in distance, our result suggests that the short Pleiades distance is not at least directly related to the young age of the cluster.

The successful launch of Gaia (Perryman et al. 2001) has opened a new era in studies of stars in the Milky Way Galaxy, which will deliver precise astrometric data for about one billion stars with more than two orders of magnitude improvement in parallax measurements than available in the past. It is hoped that Gaia will eventually help to resolve the Pleiades distance problem and will cast new light on hidden systematic errors in the *Hipparcos* parallax measurements. However, the Pleiades distance controversy has revealed a practical limit in the analysis of space-based astrometric data, which leads to demand for a careful check on the future parallax measurements. Our analysis technique based on accurate spectroscopic data can be utilized to assess the accuracy of parallax measurements by Gaia.

We thank an anonymous referee for various suggestions, which helped to improve the readability of the manuscript. We thank Courtney Epstein for her assistance in the observations. B.K. and D.A. acknowledge support provided by the National Research Foundation of Korea to the Center for Galaxy Evolution Research (No. 2010-0027910) and by Basic Science Research Program through the National Research Foundation of Korea (NRF) funded by the Ministry of Education (2010-0025122, 2015R1D1A1A09058700). This work has developed from a master's thesis conducted by B.K. under the supervision of D.A. at Ewha Womans University. J.R.S. gratefully acknowledges funding support from NASA Kepler grant NNX1AV62G. Y.S.L. acknowledges support provided by the National Research Foundation of Korea to the Center for Galaxy Evolution Research (No. 2010-0027910) and the Basic Science Research Program through the National Research Foundation of Korea (NRF) funded by the Ministry of Science, ICT & Future Planning (NRF-2015R1C1A1A02036658). D.M.T. acknowledges support from award AST-1411685 from the National Science Foundation to The Ohio State University. This research has made use of the NASA Star and Exoplanet Database (NStED), which was operated until 2011 by the California Institute of Technology, under contract with the National Aeronautics and Space Administration. This research has made use of the SIMBAD database, operated at CDS, Strasbourg, France.

REFERENCES

An, D., Terndrup, D. M., & Pinsonneault, M. H. 2007a, ApJ, 671, 1640
An, D., Terndrup, D. M., Pinsonneault, M. H., et al. 2007b, ApJ, 655, 233
An, D., Terndrup, D. M., Pinsonneault, M. H., & Lee, J.-W. 2015, ApJ, 811, 46
Anders, E., & Grevesse, N. 1989, Geochim. Cosmochim. Acta, 53, 197
Aumer, M., & Binney, J. J. 2009, MNRAS, 397, 1286
Baliunas, S., & Soon, W. 1995, ApJ, 450, 896
Belikov, A. N., Hirte, S., Meusinger, H., Piskunov, A. E., & Schilbach, E. 1998, A&A, 332, 575
Bensby, T., Feltzing, S., & Lundström, I. 2003, A&A, 410, 527
Bensby, T., Feltzing, S., & Oey, M. S. 2014, A&A, 562, AA71
Boesgaard, A. M., Roper, B. W., & Lum, M. G. 2013, ApJ, 775, 58
Butler, R. P., Marcy, G. W., Cohen, R. D., & Duncan, D. K. 1987, ApJ, 319, L19
Casagrande, L., Portinari, L., & Flynn, C. 2006, MNRAS, 373, 13
Casagrande, L., Ramírez, I., Meléndez, J., Bessell, M., & Asplund, M. 2010, A&A, 512, A54
Casagrande, L., Silva Aguirre, V., Schlesinger, K. J., et al. 2016, MNRAS, 455, 987
Castelli, F., & Kurucz, R. L. 2004, arXiv:astro-ph/0405087
Daniel, K. J., Linsky, J. L., & Gagné, M. 2002, ApJ, 578, 486
de Bruijne, J. H. J., Hoogerwerf, R., & de Zeeuw, P. T. 2001, A&A, 367, 111
Garcia Lopez, R. J., Rebolo, R., & Beckman, J. E. 1988, PASP, 100, 1489
Garcia Lopez, R. J., Rebolo, R., & Martin, E. L. 1994, A&A, 282, 518
Grevesse, N., & Sauval, A. J. 1999, A&A, 347, 348
Hobbs, L. M., & Pilachowski, C. 1986, ApJ, 311, L37
Høg, E., Fabricius, C., Makarov, V. V., et al. 2000, A&A, 355, L27
Huensch, M., Schmitt, J. H. M. M., & Voges, W. 1998, A&AS, 132, 155
Hünsch, M., Schmitt, J. H. M. M., Sterzik, M. F., & Voges, W. 1999, A&AS, 135, 319
Jeffries, R. D. 1999, MNRAS, 309, 189
Jones, B. F., Fischer, D., & Soderblom, D. R. 1999, AJ, 117, 330
Jones, B. F., Shetrone, M., Fischer, D., & Soderblom, D. R. 1996, AJ, 112, 186
Kamai, B. L., Vrba, F. J., Stauffer, J. R., & Stassun, K. G. 2014, AJ, 148, 30
Lee, Y. S., Beers, T. C., Sivarani, T., et al. 2008a, AJ, 136, 2022
Lee, Y. S., Beers, T. C., Sivarani, T., et al. 2008b, AJ, 136, 2050
Makarov, V. V. 2002, AJ, 124, 3299
Makarov, V. V. 2003, AJ, 126, 2408
Mamajek, E. E., & Hillenbrand, L. A. 2008, ApJ, 687, 1264
Mamajek, E. E., Meyer, M. R., & Liebert, J. 2002, AJ, 124, 1670
Mamajek, E. E., Meyer, M. R., & Liebert, J. 2006, AJ, 131, 2360
Markwardt, C. B. 2009, Astronomical Data Analysis Software and Systems XVIII, 411, 251
Melis, C., Reid, M. J., Mioduszewski, A. J., Stauffer, J. R., & Bower, G. C. 2014, Science, 345, 1029
Munari, U., Dallaporta, S., Siviero, A., et al. 2004, A&A, 418, L31
Narayanan, V. K., & Gould, A. 1999, ApJ, 523, 328
Noyes, R. W., Hartmann, L. W., Baliunas, S. L., Duncan, D. K., & Vaughan, A. H. 1984, ApJ, 279, 763
Pace, G. 2013, A&A, 551, L8
Pan, X., Shao, M., & Kulkarni, S. R. 2004, Nature, 427, 326
Pasquini, L., Randich, S., & Pallavicini, R. 1997, A&A, 325, 535
Paulson, D. B., Sneden, C., & Cochran, W. D. 2003, AJ, 125, 3185
Percival, S. M., Salaris, M., & Kilkenny, D. 2003, A&A, 400, 541
Perryman, M. A. C., Brown, A. G. A., Lebreton, Y., et al. 1998, A&A, 331, 81
Perryman, M. A. C., Lindegren, L., Kovalevsky, J., et al. 1997, A&A, 323, L49
Perryman, M. A. C., de Boer, K. S., Gilmore, G., et al. 2001, A&A, 369, 339
Pinsonneault, M. H., Stauffer, J., Soderblom, D. R., King, J. R., & Hanson, R. B. 1998, ApJ, 504, 170
Pinsonneault, M. H., Terndrup, D. M., Hanson, R. B., & Stauffer, J. R. 2004, ApJ, 600, 946
Portinari, L., Casagrande, L., & Flynn, C. 2010, MNRAS, 406, 1570
Pourbaix, D., Tokovinin, A. A., Batten, A. H., et al. 2004, A&A, 424, 724
Ramirez, S., Akeson, R. L., Ciardi, D., et al. 2013, American Astronomical Society Meeting Abstracts #221, 221, #334.01
Randich, S., Primas, F., Pasquini, L., & Pallavicini, R. 2002, A&A, 387, 222
Schmitt, J. H. M. M., & Liefke, C. 2004, A&A, 417, 651
Skrutskie, M. F., Cutri, R. M., Stiening, R., et al. 2006, AJ, 131, 1163
Sneden, C. A. 1973, Ph.D. Thesis
Soderblom, D. R. 2010, ARA&A, 48, 581
Soderblom, D. R., Jones, B. F., Balachandran, S., et al. 1993a, AJ, 106, 1059
Soderblom, D. R., Jones, B. F., Stauffer, J. R., & Chaboyer, B. 1995, AJ, 110, 729
Soderblom, D. R., Oey, M. S., Johnson, D. R. H., & Stone, R. P. S. 1990, AJ, 99, 595
Soderblom, D. R., Stauffer, J. R., Hudon, J. D., & Jones, B. F. 1993b, ApJS, 85, 315
Soderblom, D. R., King, J. R., Hanson, R. B., et al. 1998, ApJ, 504, 192
Soderblom, D. R., Nelan, E., Benedict, G. F., et al. 2005, AJ, 129, 1616
Spite, F., Spite, M., Peterson, R. C., & Chaffee, F. H., Jr. 1987, A&A, 171, L8
Stauffer, J. R., Hartmann, L. W., Fazio, G. G., et al. 2007, ApJS, 172, 663
Stauffer, J. R., Jones, B. F., Backman, D., et al. 2003, AJ, 126, 833
Stoughton, C., Lupton, R. H., Bernardi, M., et al. 2002, AJ, 123, 485
Taylor, B. J. 1980, AJ, 85, 242
Thorburn, J. A., Hobbs, L. M., Deliyannis, C. P., & Pinsonneault, M. H. 1993, ApJ, 415, 150
Torres, G., Fischer, D. A., Sozzetti, A., et al. 2012, ApJ, 757, 161
Valenti, J. A., & Fischer, D. A. 2005, ApJS, 159, 141 (VF05)
Valenti, J. A., & Piskunov, N. 1996, A&AS, 118, 595
Vandenberg, D. A., & Bridges, T. J. 1984, ApJ, 278, 679
van Leeuwen, F. 1999, A&A, 341, L71
van Leeuwen, F. 2005, A&A, 439, 805
van Leeuwen, F. 2007a, Hipparcos, the new reduction of the raw data (Dordrecht: Springer)
van Leeuwen, F. 2007b, A&A, 474, 653
van Leeuwen, F. 2009, A&A, 497, 209
van Leeuwen, F., & Fantino, E. 2005, A&A, 439, 791
van Leeuwen, F., & Hansen Ruiz, C. S. 1997, Hipparcos - Venice '97, 402, 689
Yanny, B., Rockosi, C., Newberg, H. J., et al. 2009, AJ, 137, 4377
York, D. G., Adelman, J., Anderson, J. E., Jr., et al. 2000, AJ, 120, 1579

TABLE 1
PHOTOMETRIC PROPERTIES OF THE KPNO SAMPLE

HIP	HD	V (mag)	$\sigma(V)$ (mag)	$B-V$ (mag)	σ_{B-V} (mag)	$V-K_s$ (mag)	σ_{V-K_s} (mag)	π[a] (arcsec)	σ_π[a] (arcsec)	M_V[b] (mag)	$\sigma(M_V)$ (mag)	Number of Obs. Spring	Number of Obs. Autumn
1674	1624	8.48	0.02	0.80	0.02	2.62	0.03	31.54	0.96	5.97	0.11	···	2
4907	5996	7.66	0.02	0.75	0.02	1.76	0.03	39.20	0.56	5.63	0.10	···	1
5313	6664	7.78	0.02	0.61	0.02	1.53	0.03	31.79	1.66	5.29	0.13	···	2
5521	6963	7.66	0.02	0.73	0.02	1.72	0.03	36.95	0.79	5.50	0.10	···	1
9172	11926	7.57	0.02	0.66	0.02	···	···	31.99	0.86	5.09	0.06	···	1
9829	12846	6.89	0.02	0.65	0.02	1.59	0.03	43.89	0.57	5.10	0.04	···	2
10276	13483	8.46	0.02	0.77	0.03	1.87	0.03	31.58	1.11	5.96	0.11	···	2
10629	13783	8.29	0.02	0.69	0.02	1.71	0.03	25.37	0.93	5.31	0.08	···	2
11507	15361	8.60	0.02	0.66	0.03	1.62	0.03	21.44	0.89	5.25	0.04	···	2
12685	16702	8.29	0.02	0.60	0.02	1.58	0.03	20.44	0.93	4.84	0.11	···	1
13771	18123	8.80	0.02	0.67	0.03	1.71	0.03	19.87	1.15	5.29	0.10	···	2
14241	19034	8.08	0.02	0.67	0.03	1.70	0.03	28.52	0.97	5.36	0.04	···	2
14300	18916	7.99	0.02	0.68	0.02	1.59	0.03	27.97	0.94	5.22	0.07	···	2
15062	20065	8.13	0.02	0.62	0.02	1.58	0.03	25.52	0.90	5.16	0.14	···	1
15442	20619	7.03	0.02	0.65	0.02	1.56	0.03	39.64	0.74	5.02	0.15	···	1
17265	23065	8.27	0.02	0.74	0.03	1.89	0.04	32.89	0.74	5.86	0.09	···	1
18324	24238	7.82	0.02	0.86	0.02	2.13	0.03	47.60	0.84	6.21	0.10	···	1
20722	27857	8.05	0.02	0.64	0.02	1.55	0.03	24.12	0.87	4.96	0.11	···	1
21276	28495	7.76	0.02	0.78	0.02	2.01	0.03	39.37	1.11	5.73	0.11	···	1
21571	29021	7.76	0.02	0.69	0.02	1.68	0.03	33.07	0.77	5.36	0.04	···	2
21832[c]	29587	7.28	0.02	0.61	0.02	1.63	0.03	36.30	0.87	5.08	0.11	···	1
22175	30286	7.83	0.02	0.68	0.02	1.61	0.03	30.53	0.82	5.25	0.02	···	1
23431	32237	8.19	0.02	0.78	0.02	1.86	0.03	33.33	1.42	5.80	0.03	···	1
23786	32850	7.74	0.02	0.81	0.02	2.00	0.03	42.25	0.92	5.87	0.04	···	1
26505	37008	7.74	0.02	0.84	0.02	2.11	0.03	49.59	0.72	6.21	0.12	···	2
30862	45391	7.14	0.02	0.63	0.02	1.57	0.03	40.70	0.62	5.19	0.09	···	2
44259[c]	77065	8.78	0.02	0.83	0.04	2.15	0.03	31.54	1.05	6.28	0.05	2	···
44262	77052	8.84	0.02	0.64	0.04	1.55	0.03	16.75	1.11	4.96	0.04	2	···
52278	92320	8.38	0.02	0.69	0.02	1.57	0.03	23.79	0.78	5.26	0.07	1	···
52470	92786	7.98	0.02	0.78	0.02	1.85	0.03	37.54	0.76	5.86	0.10	1	···
54906	97658	7.76	0.02	0.84	0.02	2.03	0.03	47.36	0.75	6.14	0.14	1	···
55210	98281	7.29	0.02	0.75	0.02	1.83	0.04	46.37	0.64	5.62	0.12	2	···
56092	238006	9.69	0.02	0.95	0.04	2.19	0.03	25.17	1.55	6.69	0.02	2	···
56337	100310	8.82	0.02	0.73	0.03	1.73	0.03	22.79	1.16	5.61	0.05	2	···
56837	101227	8.44	0.02	0.68	0.02	···	···	26.34	0.88	5.54	0.14	1	···
57939	103095	6.45	0.02	0.75	0.02	2.08	0.03	109.98	0.41	6.66	0.12	2	···
57992	103126	8.29	0.02	0.74	0.02	1.84	0.03	32.98	0.56	5.88	0.11	1	···
58949	104988	8.17	0.02	0.74	0.02	1.85	0.03	30.97	0.85	5.63	0.12	1	···
60074	107146	7.04	0.02	0.61	0.02	1.50	0.03	36.42	0.53	4.84	0.06	2	···
60268[c]	107582	8.25	0.02	0.61	0.02	1.65	0.03	24.48	0.62	5.20	0.03	1	···
63322	112733B	9.31	0.02	0.87	0.04	2.43	0.03	24.64	1.67	6.27	0.07	2	···
63346	112956	8.06	0.02	0.69	0.02	1.74	0.03	30.00	0.56	5.44	0.08	1	···
63636	113319	7.51	0.02	0.65	0.02	1.54	0.03	32.15	0.56	5.05	0.07	2	···
64076	114216	8.50	0.02	0.61	0.02	1.55	0.03	20.40	0.62	5.05	0.07	2	···
64131	114172	8.56	0.02	0.62	0.02	1.56	0.03	21.56	0.88	5.23	0.13	2	···
65165	116272	8.48	0.02	0.77	0.02	1.78	0.03	27.05	0.63	5.64	0.08	1	···
65352	116442	7.03	0.02	0.81	0.02	1.94	0.03	64.73	1.33	6.09	0.13	2	···
65355	116443	7.29	0.02	0.88	0.02	2.06	0.03	61.94	1.34	6.25	0.12	1	···
65935	···	9.63	0.02	0.90	0.04	2.19	0.03	23.45	1.35	6.48	0.02	2	···
66509	118659	8.83	0.02	0.65	0.03	1.70	0.03	19.64	1.13	5.29	0.15	1	···
67211	119932	9.31	0.03	0.95	0.05	2.40	0.03	30.75	1.42	6.75	0.12	2	···
67282	120067	8.70	0.02	0.83	0.03	1.96	0.03	28.91	0.97	6.00	0.12	2	···
67773	121131	8.36	0.02	0.81	0.02	2.01	0.03	34.41	1.22	6.04	0.04	1	···
67904	121320	7.88	0.02	0.70	0.02	1.63	0.03	31.73	0.71	5.38	0.12	3	···
70253	126244	8.23	0.02	0.61	0.02	1.59	0.03	24.27	0.64	5.16	0.13	1	···
70319	126053	6.27	0.02	0.63	0.02	1.63	0.03	58.17	0.52	5.09	0.05	3	···
71720	128985	9.17	0.02	0.86	0.04	1.95	0.03	24.74	1.37	6.14	0.06	1	···
72577	130871	9.06	0.02	0.95	0.04	2.34	0.03	33.18	1.85	6.67	0.13	2	···
72663	131025	8.48	0.02	0.68	0.03	1.64	0.03	23.25	1.30	5.31	0.10	1	···
72703	131179	8.36	0.02	0.70	0.03	1.66	0.03	26.08	0.87	5.44	0.03	1	···
73005	132142	7.76	0.02	0.81	0.02	1.96	0.03	42.75	0.45	5.91	0.08	1	···
73138	132051	8.65	0.02	0.77	0.03	1.94	0.03	29.25	1.60	5.98	0.08	1	···
73677	133564	8.80	0.02	0.63	0.02	1.54	0.03	18.58	0.74	5.15	0.10	1	···
73845	133910	9.10	0.02	0.63	0.03	1.56	0.03	15.36	0.90	5.03	0.09	1	···
74126	134251	8.88	0.02	0.66	0.03	1.65	0.04	20.33	1.09	5.42	0.13	1	···
74396	135144	8.59	0.02	0.87	0.02	2.12	0.03	33.27	0.76	6.20	0.10	1	···
75059	136563	8.57	0.02	0.67	0.02	1.53	0.03	20.50	1.04	5.12	0.06	1	···
75370	137826	8.74	0.02	0.67	0.03	1.76	0.03	20.43	0.73	5.30	0.09	1	···
75446	137336	8.98	0.02	0.73	0.03	1.73	0.03	22.37	1.15	5.73	0.14	1	···
75703	138134	9.05	0.02	0.75	0.03	1.83	0.03	23.14	0.79	5.87	0.13	1	···
76058	138442	8.73	0.02	0.64	0.03	1.59	0.03	19.55	1.10	5.18	0.08	2	···
76130	···	8.98	0.02	0.61	0.03	1.47	0.03	15.15	0.94	4.88	0.08	1	···
76330	139194	8.62	0.02	0.86	0.02	2.12	0.04	33.50	0.83	6.25	0.11	1	···
76674	139837	9.00	0.02	0.74	0.03	1.82	0.03	20.37	1.05	5.55	0.12	1	···
77810	142229	8.08	0.02	0.62	0.02	1.47	0.03	24.53	1.25	5.03	0.15	1	···

TABLE 1 — *Continued*

HIP	HD	V (mag)	$\sigma(V)$ (mag)	$B-V$ (mag)	σ_{B-V} (mag)	$V-K_s$ (mag)	σ_{V-K_s} (mag)	π[a] (arcsec)	σ_π[a] (arcsec)	M_V[b] (mag)	$\sigma(M_V)$ (mag)	Number of Obs. Spring	Number of Obs. Autumn
78028	···	8.64	0.02	0.63	0.02	1.54	0.03	18.30	0.81	4.95	0.08	1	···
78241	143291	8.01	0.02	0.76	0.02	1.91	0.03	38.11	0.76	5.91	0.08	1	···
78336	143295	9.09	0.02	0.88	0.04	2.25	0.03	30.27	1.10	6.49	0.14	1	···
78550	143990	8.75	0.02	0.67	0.02	1.70	0.03	22.61	0.92	5.52	0.12	1	···
78775	144579	6.65	0.02	0.74	0.02	1.90	0.03	68.88	0.33	5.84	0.13	1	···
78923	144873	8.54	0.02	0.69	0.02	1.62	0.03	21.65	0.81	5.21	0.05	1	···
79629	146868	7.69	0.02	0.65	0.02	1.69	0.03	32.54	0.44	5.25	0.13	2	···
80243	148226	8.75	0.02	0.79	0.03	1.97	0.03	26.52	0.61	5.87	0.11	1	···
80262	147750	8.44	0.02	0.72	0.02	1.74	0.03	25.20	0.92	5.44	0.06	1	···
81186	149929	9.34	0.02	0.88	0.04	2.14	0.03	26.10	0.78	6.42	0.12	2	···
81288	150172	8.95	0.02	0.88	0.03	2.29	0.03	32.19	0.90	6.49	0.08	1	···
81605	150510	8.63	0.02	0.72	0.02	1.73	0.03	22.41	0.83	5.38	0.13	1	···
81831	···	8.91	0.02	0.73	0.03	1.68	0.03	24.33	1.18	5.84	0.08	1	···
82120	151192	8.23	0.02	0.68	0.02	1.71	0.03	27.40	1.02	5.42	0.05	2	···
82210	152012	8.40	0.02	0.67	0.02	1.56	0.03	22.91	0.75	5.20	0.06	1	···
82388	151798	7.95	0.02	0.61	0.02	1.47	0.03	23.78	0.85	4.83	0.13	2	···
82644	152793	8.68	0.02	0.64	0.02	1.56	0.03	19.65	0.67	5.15	0.08	2	···
82712	···	8.52	0.02	0.70	0.02	1.78	0.03	25.44	0.95	5.55	0.10	1	···
83141	···	9.37	0.02	0.96	0.04	2.36	0.03	28.55	0.97	6.65	0.15	2	···
83276	153631	7.12	0.02	0.62	0.02	1.54	0.03	36.52	1.36	4.93	0.05	2	···
83500	···	8.82	0.02	0.62	0.03	1.46	0.03	16.29	0.81	4.88	0.04	1	···
84520	156728	8.03	0.02	0.64	0.02	1.53	0.03	24.85	0.59	5.01	0.04	1	···
85235	158633	6.43	0.02	0.76	0.02	1.92	0.03	78.11	0.30	5.89	0.14	2	···
85653	159062	7.22	0.02	0.74	0.02	1.83	0.03	44.91	0.50	5.48	0.15	1	···
86568	···	9.75	0.03	0.74	0.05	1.91	0.03	17.12	1.01	5.92	0.14	2	···
86765	161098	7.67	0.02	0.67	0.02	1.66	0.04	33.14	0.75	5.27	0.02	1	···
87089	161848	8.91	0.02	0.80	0.03	2.09	0.03	26.29	1.03	6.01	0.04	1	···
88166	···	9.22	0.02	0.70	0.03	1.79	0.03	20.52	1.33	5.78	0.12	2	···
88972	166620	6.40	0.02	0.87	0.02	2.17	0.03	90.71	0.30	6.19	0.15	1	···
90355[c]	169822	7.83	0.02	0.69	0.02	1.75	0.03	34.63	1.39	5.53	0.11	1	···
90415	···	9.88	0.03	0.91	0.05	2.16	0.03	20.56	0.99	6.44	0.10	3	···
90708	···	9.13	0.02	0.64	0.03	1.54	0.03	15.31	0.83	5.06	0.08	1	···
91364	172393	8.33	0.02	0.84	0.02	2.05	0.03	35.60	0.66	6.09	0.06	1	···
91381	172310	8.40	0.02	0.71	0.02	1.76	0.03	26.86	1.03	5.54	0.12	1	···
91438	172051	5.86	0.02	0.66	0.02	···	···	76.42	0.46	5.28	0.08	···	1
91605	···	8.57	0.02	0.93	0.03	2.35	0.03	42.48	1.11	6.71	0.05	1	···
91614	336669	8.99	0.02	0.69	0.03	1.62	0.03	18.00	0.98	5.27	0.06	1	···
91905	173665	8.54	0.02	0.75	0.03	1.81	0.03	27.81	0.54	5.76	0.09	2	···
92388	229635	8.58	0.02	0.72	0.03	1.86	0.03	27.29	0.83	5.76	0.06	1	···
92569	174719	7.51	0.02	0.68	0.02	1.66	0.03	35.20	0.62	5.24	0.06	1	···
93195	176157	8.37	0.02	0.82	0.02	1.98	0.03	32.41	0.97	5.92	0.10	···	1
93731	177745	8.54	0.02	0.79	0.02	1.92	0.03	31.47	1.01	6.03	0.09	1	···
94582	···	9.54	0.02	0.78	0.04	1.83	0.03	18.09	0.68	5.82	0.14	2	···
95727	231510	9.01	0.02	0.77	0.03	1.89	0.03	23.76	1.46	5.89	0.05	3	···
96100	185144	4.69	0.02	0.80	0.02	···	···	173.77	0.18	5.89	0.13	1	···
96344	···	9.75	0.03	0.66	0.05	1.52	0.03	12.52	0.75	5.24	0.12	2	···
96634	···	9.13	0.02	0.79	0.03	2.01	0.03	21.89	0.84	5.83	0.11	2	···
96735	···	9.20	0.02	0.87	0.03	2.21	0.03	26.09	0.91	6.28	0.12	2	···
97640[c]	226099	8.02	0.02	0.78	0.02	2.14	0.03	35.20	0.61	5.75	0.13	1	···
97668	187645	9.58	0.05	0.90	0.08	2.26	0.05	26.95	1.85	6.74	0.11	···	2
98288[c]	190061	9.27	0.02	0.62	0.03	1.58	0.03	13.26	0.68	4.88	0.07	2	···
98413	189242	9.23	0.02	0.90	0.03	2.26	0.03	27.32	1.43	6.42	0.04	···	2
98559	189540	9.30	0.02	0.70	0.03	1.72	0.03	17.12	1.10	5.47	0.11	···	2
98677	190067	7.15	0.02	0.74	0.02	1.83	0.03	52.70	0.65	5.76	0.15	1	···
98792	190404	7.27	0.02	0.84	0.02	2.16	0.03	63.42	0.57	6.28	0.02	1	2
98965	190609	8.63	0.02	0.72	0.02	1.75	0.03	25.04	1.29	5.63	0.05	1	···
99355	192139	8.74	0.02	0.89	0.03	2.21	0.03	35.68	0.83	6.50	0.09	1	···
99774	···	9.12	0.02	0.60	0.03	1.59	0.03	17.01	0.65	5.28	0.14	2	···
99965[c]	193216	8.16	0.02	0.76	0.02	1.75	0.03	32.51	0.55	5.72	0.12	1	···
100259	193554	8.27	0.02	0.62	0.02	1.60	0.03	21.64	0.77	4.94	0.03	1	···
101579	196124	8.94	0.02	0.95	0.03	2.41	0.03	34.91	1.20	6.65	0.03	···	2
101997	196761	6.37	0.02	0.72	0.02	···	···	69.54	0.40	5.58	0.13	···	1
102290	197300	8.65	0.02	0.60	0.03	1.45	0.03	17.54	0.96	4.87	0.10	···	2
102521	197818	7.66	0.02	0.61	0.02	1.51	0.03	27.83	0.78	4.88	0.04	···	1
103611	199803	8.57	0.02	0.68	0.03	1.61	0.03	22.15	1.03	5.29	0.12	2	···
103895	···	9.17	0.02	0.69	0.03	1.77	0.03	19.70	0.95	5.64	0.15	2	···
103896	200297	8.55	0.02	0.63	0.03	1.56	0.03	21.42	1.10	5.21	0.12	···	2
104375	202123	8.68	0.02	0.87	0.03	2.10	0.03	32.10	0.63	6.21	0.13	1	···
104733	202108	7.33	0.02	0.65	0.02	1.58	0.03	37.13	0.56	5.18	0.03	1	1
106231	···	9.25	0.02	0.99	0.04	2.86	0.03	40.32	1.06	7.27	0.07	···	2
106949	···	8.97	0.02	0.65	0.02	1.66	0.03	18.89	1.00	5.36	0.11	2	···
107038	207897	8.40	0.02	0.87	0.02	2.09	0.03	35.49	0.48	6.15	0.05	1	···
107700	208002	8.98	0.02	0.86	0.03	2.12	0.03	27.20	0.78	6.15	0.08	1	···
108774	209393	7.94	0.02	0.70	0.02	1.62	0.03	29.61	0.82	5.30	0.05	1	···
108947	209599	8.39	0.02	0.79	0.03	1.93	0.03	31.24	0.96	5.86	0.07	1	···
109310	210323	8.41	0.02	0.62	0.02	1.45	0.03	19.69	0.97	4.88	0.07	···	2

TABLE 1 — *Continued*

HIP	HD	V (mag)	$\sigma(V)$ (mag)	$B-V$ (mag)	σ_{B-V} (mag)	$V-K_s$ (mag)	σ_{V-K_s} (mag)	π[a] (arcsec)	σ_π[a] (arcsec)	M_V[b] (mag)	$\sigma(M_V)$ (mag)	Number of Obs. Spring	Autumn
110508	212291	7.91	0.02	0.70	0.02	1.64	0.03	30.07	0.60	5.30	0.06	1	···
111883	···	8.76	0.02	0.89	0.03	2.18	0.03	32.84	0.97	6.34	0.09	···	2
111888	214683	8.48	0.02	0.90	0.03	2.34	0.03	41.51	0.77	6.57	0.15	1	···
111977	215065	7.46	0.02	0.63	0.02	1.61	0.03	34.10	0.47	5.12	0.14	1	···
112245	215500	7.50	0.02	0.73	0.02	1.77	0.03	39.76	0.56	5.50	0.05	1	···
112870	216259	8.29	0.02	0.87	0.02	2.21	0.03	46.97	1.01	6.65	0.09	···	1
113231	216777	8.00	0.02	0.65	0.02	1.64	0.03	27.21	1.12	5.17	0.03	1	···
113884	217924	7.22	0.02	0.62	0.02	1.57	0.03	38.37	2.11	5.14	0.05	1	2
113989	218209	7.50	0.02	0.64	0.02	1.70	0.03	33.84	0.38	5.15	0.06	1	···
114340	218614	8.78	0.02	0.67	0.03	1.57	0.03	19.23	1.09	5.20	0.08	···	2
114385	218739	7.14	0.02	0.65	0.02	1.47	0.03	40.08	2.19	5.15	0.06	···	1
115194	219953	8.86	0.02	0.79	0.03	2.11	0.03	30.20	1.04	6.26	0.09	···	2
115411	220293	8.74	0.02	0.67	0.03	1.85	0.03	22.58	1.04	5.51	0.08	···	1
115445	220339	7.79	0.02	0.90	0.03	2.19	0.03	52.27	0.86	6.38	0.03	···	1
116005	221239	8.35	0.02	0.88	0.02	2.21	0.03	38.64	0.86	6.29	0.04	···	3
116410	221822	8.40	0.02	0.74	0.03	1.76	0.03	26.87	1.35	5.54	0.14	···	1
118207	224540	8.37	0.02	0.64	0.02	1.55	0.03	22.83	0.58	5.16	0.13	···	2
118251	···	8.15	0.02	0.64	0.02	1.57	0.03	23.86	0.65	5.04	0.09	···	1
118278	224619	7.48	0.02	0.74	0.02	1.77	0.04	39.84	0.78	5.48	0.07	···	1

[a] Parallaxes and parallax errors from the revised *Hipparcos* catalog (van Leeuwen 2007a,b).

[b] Absolute magnitude computed from the *Hipparcos* parallax.

[c] A spectroscopic binary listed in the 9^{th} catalogue of spectroscopic binary orbits (Pourbaix et al. 2004, `http://sb9.astro.ulb.ac.be`).

TABLE 2
STELLAR PARAMETERS DERIVED USING MOOG

HIP	$T_{\rm eff}$ (K)	$\log g$	[Fe/H]	ξ (km s^{-1})	[Fe/H]$_{\rm corr}$[a]	σ([Fe/H])
4907	5405	4.34	–0.16	1.2	–0.09	0.019
5313[b]	5881	4.05	–0.29	1.3	–0.22	0.017
5521	5398	4.00	–0.29	1.1	–0.22	0.009
9172	5638	4.04	–0.13	1.4	–0.06	0.009
9829	5795	4.29	–0.22	1.1	–0.14	0.020
10276[b]	5368	4.42	–0.25	1.2	–0.18	0.016
15442	5760	4.18	–0.27	1.3	–0.20	0.026
17265	5339	4.23	–0.69	1.3	–0.62	0.026
18324	5216	4.01	–0.55	1.4	–0.48	0.030
21276	5448	4.27	–0.17	1.4	–0.10	0.024
21571	5636	4.36	–0.30	1.3	–0.23	0.016
21832	5609	4.17	–0.67	1.3	–0.60	0.026
22175	5765	4.28	–0.16	1.4	–0.09	0.025
23786	5261	4.13	–0.27	1.2	–0.20	0.023
26505	4948	4.10	–0.60	1.0	–0.53	0.015
30862	5663	4.15	–0.56	1.2	–0.49	0.010
52470	5367	4.34	–0.46	1.1	–0.39	0.028
54906	5403	4.31	–0.26	1.3	–0.19	0.032
55210	5314	3.81	–0.36	1.1	–0.28	0.018
56092[b]	5030	4.33	–0.44	1.2	–0.37	0.020
57939	5072	3.77	–1.42	1.1	–1.35	0.021
57992	5431	4.36	–0.43	1.0	–0.36	0.030
58949	5291	4.14	–0.32	0.9	–0.25	0.024
60074	5915	3.92	–0.12	1.6	–0.05	0.019
60268	5678	3.98	–0.60	0.8	–0.53	0.031
63346	5779	4.36	–0.45	1.6	–0.38	0.031
63636	5739	3.90	–0.25	1.7	–0.18	0.028
65165	5431	4.13	–0.13	1.2	–0.06	0.026
65352	5178	3.99	–0.48	1.1	–0.40	0.018
65355	5054	4.13	–0.42	1.0	–0.35	0.026
67904	5304	4.37	–0.44	1.1	–0.37	0.014
70253	5550	3.80	–0.66	1.0	–0.59	0.021
70319	5608	3.88	–0.46	1.2	–0.39	0.014
71720[b]	5285	4.50	–0.24	1.2	–0.17	0.029
73005	5219	4.33	–0.44	0.9	–0.37	0.025
73138[b]	5327	4.39	–0.07	1.0	+0.00	0.027
73845[b]	5620	3.50	–0.60	0.8	–0.53	0.025
74126[b]	5805	4.36	–0.02	1.2	+0.05	0.031
74396	5166	4.44	–0.23	1.2	–0.16	0.027
75446[b]	5519	4.16	–0.15	1.1	–0.08	0.026
76330	5101	4.15	–0.31	1.5	–0.24	0.029
77810[b]	5949	4.07	+0.01	1.2	+0.08	0.023

TABLE 2 — *Continued*

HIP	$T_{\rm eff}$ (K)	$\log g$	[Fe/H]	ξ (km s^{-1})	[Fe/H]$_{\rm corr}$[a]	σ([Fe/H])
78241	5318	3.86	–0.46	1.1	–0.39	0.029
78336[b]	5053	4.32	–0.05	1.3	+0.02	0.025
78775	5233	3.87	–0.76	1.0	–0.69	0.021
79629	5663	4.19	–0.35	1.3	–0.28	0.017
80243	5356	4.14	–0.10	1.5	–0.03	0.026
81186	5031	4.19	–0.45	1.2	–0.37	0.017
81288	4934	4.33	–0.91	0.8	–0.84	0.019
81831[b]	5509	4.16	–0.37	1.2	–0.30	0.025
84520	5708	3.90	–0.29	1.3	–0.22	0.023
85235	5263	4.21	–0.51	1.0	–0.43	0.015
85653	5465	4.43	–0.48	1.3	–0.41	0.018
86765	5625	4.21	–0.27	1.1	–0.20	0.025
88972	5048	4.26	–0.35	1.1	–0.28	0.027
91364	5268	4.11	–0.43	1.3	–0.36	0.028
91438	5605	4.25	–0.31	1.2	–0.24	0.020
91605	5026	4.04	–0.52	1.3	–0.45	0.026
91905	5396	4.20	–0.42	1.2	–0.34	0.019
92569	5651	3.29	–0.27	1.3	–0.20	0.025
93195	5191	4.10	–0.18	1.2	–0.11	0.025
96100	5438	4.25	–0.28	1.4	–0.21	0.026
97668[b]	5016	4.41	–0.29	1.2	–0.22	0.021
98677	5415	4.38	–0.36	0.9	–0.29	0.022
98792	5104	4.46	–0.70	1.1	–0.63	0.013
99355	5227	4.27	–0.49	1.7	–0.42	0.029
99965	5730	3.96	+0.08	1.4	+0.15	0.026
101997	5511	4.24	–0.30	1.1	–0.23	0.027
102521	5688	4.01	–0.35	1.3	–0.28	0.019
104375	5117	4.38	–0.41	0.9	–0.34	0.024
104733	5774	4.09	–0.25	1.3	–0.18	0.018
107038	5277	4.28	–0.22	1.4	–0.15	0.028
107700	5253	4.53	–0.34	1.3	–0.27	0.028
108774	5653	4.06	–0.25	1.4	–0.18	0.026
110508	5714	3.55	–0.19	1.4	–0.12	0.026
111883	5021	4.36	–0.44	1.2	–0.37	0.013
111888	4904	4.44	–0.40	1.2	–0.33	0.032
111977	5686	4.27	–0.54	1.3	–0.47	0.024
112245	5631	4.09	–0.26	1.6	–0.19	0.026
112870	4930	4.30	–0.74	0.8	–0.67	0.026
113989	5607	4.07	–0.58	1.4	–0.51	0.025
114385[b]	5906	4.16	+0.03	1.5	+0.10	0.023
115445	5115	4.33	–0.40	1.3	–0.33	0.028
116005	5024	4.35	–0.28	1.2	–0.21	0.015
118207	5700	4.32	–0.33	1.1	–0.25	0.012
118251	5693	3.75	–0.51	1.3	–0.44	0.029
118278	5604	3.87	–0.21	1.4	–0.14	0.031

[a] Corrected to match the metallicity scale of VF05 (see text).

[b] Stars with less accurate parallax measurements ($\sigma_\pi/\pi > 3\%$), but included as having larger magnitude excesses (ΔM_V) than the Pleiades.

TABLE 3
ATOMIC LINE LIST

Element	Ion	Wavelength (Å)	E.P. (eV)	$\log gf$
Fe	1	5775.08	4.22	−1.30
Fe	1	5809.22	3.88	−1.74
Fe	1	5849.69	3.69	−2.89
Fe	1	5852.22	4.55	−1.23
Fe	1	5855.08	4.61	−1.48
Fe	1	5856.09	4.29	−1.33
Fe	1	5858.78	4.22	−2.16
Fe	1	5859.59	4.55	−0.30
Fe	1	5861.11	4.28	−2.45
Fe	1	5862.36	4.55	−0.06
Fe	1	6027.05	4.08	−1.09
Fe	1	6127.90	4.14	−1.40
Fe	1	6151.62	2.18	−3.27
Fe	1	6157.73	4.08	−1.16
Fe	1	6159.38	4.61	−1.97
Fe	1	6165.37	4.14	−1.47
Fe	1	6173.34	2.22	−2.88
Fe	1	6180.20	2.73	−2.59
Fe	1	6213.44	2.22	−2.48
Fe	1	6219.28	2.20	−2.42
Fe	1	6226.74	3.88	−2.12
Fe	1	6229.23	2.84	−2.87
Fe	1	6240.65	2.22	−3.17
Fe	1	6270.23	2.86	−2.61
Fe	1	6322.69	2.59	−2.43
Fe	1	6335.34	2.20	−2.18
Fe	1	6344.15	2.43	−2.92
Fe	1	6380.75	4.19	−1.38
Fe	1	6481.88	2.28	−2.96
Fe	1	6498.94	0.96	−4.70
Fe	1	6627.56	4.55	−1.58
Fe	1	6703.57	2.76	−3.06
Fe	1	6750.15	2.42	−2.62
Fe	1	7107.46	4.19	−1.34
Fe	1	7127.57	4.99	−1.36
Fe	1	7130.92	4.22	−0.69
Fe	1	7132.99	4.08	−1.63
Fe	2	6149.23	3.89	−2.84
Fe	2	6247.55	3.89	−2.43
Fe	2	6456.39	3.90	−2.19
Fe	2	6516.08	2.89	−3.43
Fe	2	7224.46	3.89	−3.36

TABLE 4
SYSTEMATIC ERRORS IN ABUNDANCE MEASUREMENTS FROM MOOG ANALYSIS

Ion	$\Delta T_{\rm eff}$ ± 100 K	$\Delta \log g$ ± 0.3 dex	Δ [Fe/H] ± 0.1 dex	$\Delta\xi$ ± 0.2 km s^{-1}
Fe I	± 0.06	∓ 0.01	± 0.01	∓ 0.04
Fe II	∓ 0.06	± 0.14	± 0.02	∓ 0.04

TABLE 5
COMPARISONS BETWEEN VARIOUS SPECTROSCOPIC PARAMETER ESTIMATES

Comparison	$\langle\Delta T_{\rm eff}\rangle$ (K)	$\langle\Delta \log g\rangle$	$\langle\Delta$[Fe/H]$\rangle$	$N_{\rm star}$
MOOG – VF05	$+53 \pm 10$	-0.45 ± 0.08	-0.07 ± 0.01	30
MOOG – C10	$+32 \pm 11$	-0.35 ± 0.12	-0.02 ± 0.01	9
SMT3 – MOOG	$+37 \pm 4$	$+0.35 \pm 0.04$	$+0.16 \pm 0.02$	74
SMT3 – SMT2	$+51 \pm 4$	$+0.09 \pm 0.01$	$+0.03 \pm 0.00$	170
SMT3 – VF05	$+85 \pm 14$	-0.10 ± 0.02	$+0.07 \pm 0.01$	36
SMT3 – C10	$+84 \pm 25$	-0.08 ± 0.02	$+0.14 \pm 0.04$	11

NOTE. — All comparisons made using original metallicity estimates.

TABLE 6
STELLAR PARAMETERS DERIVED USING SMT

HIP	SMT3							SMT2					
	$T_{\rm eff}$ (K)	$\sigma(T_{\rm eff})$ (K)	$\log g$	$\sigma(\log g)$	[Fe/H]	σ([Fe/H])	[Fe/H]$_{\rm corr}$[a]	$T_{\rm eff}$ (K)	$\sigma(T_{\rm eff})$ (K)	$\log g$	$\sigma(\log g)$	[Fe/H]	σ([Fe/H])
1674	5127	71	4.45	0.054	−0.31	0.019	−0.38	5248	37	4.67	0.011	−0.24	0.009
4907	5528	24	4.67	0.128	−0.01	0.070	−0.09	5429	57	4.54	0.016	−0.07	0.013
5313	5865	72	4.49	0.053	−0.18	0.021	−0.26	5839	47	4.44	0.011	−0.19	0.010
5521	5708	48	4.81	0.133	−0.02	0.062	−0.09	5477	58	4.42	0.029	−0.17	0.015
9172	5670	54	4.58	0.089	+0.01	0.072	−0.06	5743	69	4.61	0.015	+0.05	0.014
9829	5634	31	4.11	0.030	−0.26	0.012	−0.34	5687	44	4.19	0.009	−0.23	0.009
10276	5465	18	4.67	0.125	−0.06	0.065	−0.13	5360	40	4.48	0.013	−0.13	0.011
10629	5635	26	4.34	0.033	−0.42	0.023	−0.49	5493	43	4.12	0.011	−0.54	0.011
11507	5662	39	4.34	0.037	−0.05	0.055	−0.12	5720	45	4.39	0.010	−0.02	0.009
12685	5856	122	4.58	0.137	−0.11	0.069	−0.19	5871	67	4.59	0.015	−0.10	0.014
13771	5595	19	4.24	0.021	−0.23	0.016	−0.31	5640	43	4.31	0.009	−0.20	0.007
14241	5509	9	4.16	0.014	−0.44	0.027	−0.51	5577	43	4.20	0.010	−0.39	0.009
14300	5775	54	4.52	0.060	−0.14	0.033	−0.21	5578	42	4.17	0.016	−0.26	0.011
15062	5754	61	4.24	0.032	−0.32	0.016	−0.39	5767	65	4.27	0.023	−0.31	0.014
15442	5803	84	4.49	0.081	−0.12	0.052	−0.19	5711	64	4.34	0.017	−0.17	0.013
17265	5271	80	4.29	0.045	−0.58	0.100	−0.66	5326	59	4.36	0.012	−0.54	0.012
18324	4991	150	4.30	0.059	−0.42	0.044	−0.49	5058	50	4.39	0.015	−0.37	0.013
20722	5742	86	4.39	0.101	+0.05	0.112	−0.03	5799	70	4.53	0.015	+0.08	0.013
21276	5477	14	4.68	0.156	+0.00	0.094	−0.08	5357	56	4.55	0.016	−0.07	0.014
21571	5632	31	4.41	0.044	−0.16	0.033	−0.23	5569	42	4.31	0.009	−0.21	0.009
21832	5757	84	4.32	0.075	−0.47	0.051	−0.54	5740	67	4.31	0.012	−0.47	0.010
22175	5661	53	4.43	0.075	−0.08	0.067	−0.15	5650	63	4.41	0.014	−0.08	0.014
23431	5450	24	4.40	0.069	−0.43	0.048	−0.51	5227	59	4.11	0.016	−0.60	0.017
23786	5423	24	4.71	0.105	−0.04	0.052	−0.11	5269	56	4.49	0.017	−0.13	0.015
26505	5054	73	4.39	0.033	−0.42	0.026	−0.50	5117	36	4.48	0.011	−0.38	0.010
30862	5676	37	4.13	0.034	−0.48	0.040	−0.55	5690	46	4.15	0.010	−0.48	0.010
44259	5210	52	4.69	0.072	−0.29	0.018	−0.36	5147	36	4.59	0.010	−0.32	0.010
44262	5743	58	4.41	0.047	+0.03	0.075	−0.05	5791	51	4.48	0.010	+0.05	0.008
52278	5671	45	4.18	0.029	−0.41	0.032	−0.48	5505	62	4.00	0.024	−0.54	0.016
52470	5397	32	4.44	0.068	−0.38	0.027	−0.45	5242	55	4.20	0.016	−0.49	0.014
54906	5325	63	4.63	0.144	−0.15	0.054	−0.22	5133	51	4.37	0.015	−0.29	0.016
55210	5552	15	4.58	0.070	−0.10	0.035	−0.17	5401	40	4.34	0.012	−0.21	0.011
56092	5096	104	4.69	0.110	−0.19	0.044	−0.27	4850	32	4.31	0.014	−0.36	0.012
56337	5560	20	4.60	0.072	−0.05	0.046	−0.12	5488	43	4.41	0.016	−0.09	0.010
56837	5569	21	4.37	0.044	−0.29	0.014	−0.36	5571	60	4.38	0.016	−0.28	0.015
57939	5147	69	4.47	0.067	−1.31	0.195	−1.39	5141	55	4.46	0.010	−1.32	0.010
57992	5496	13	4.47	0.059	−0.30	0.013	−0.37	5380	57	4.30	0.016	−0.38	0.015
58949	5332	54	4.37	0.072	−0.23	0.029	−0.30	5444	57	4.55	0.016	−0.15	0.015
60074	5842	68	4.59	0.079	−0.03	0.054	−0.10	5869	49	4.62	0.010	−0.02	0.010
60268	5607	24	4.16	0.017	−0.67	0.069	−0.74	5724	69	4.34	0.015	−0.59	0.014
63322	5156	88	4.63	0.094	−0.03	0.060	−0.10	5142	38	4.63	0.010	−0.04	0.010
63346	5589	36	4.29	0.035	−0.42	0.048	−0.49	5484	61	4.12	0.015	−0.50	0.015
63636	5752	90	4.53	0.119	−0.03	0.091	−0.11	5725	64	4.46	0.015	−0.04	0.015
64076	5802	64	4.38	0.043	−0.16	0.031	−0.23	5843	46	4.46	0.011	−0.13	0.010
64131	5625	28	3.95	0.044	−0.65	0.079	−0.72	5705	48	4.09	0.010	−0.58	0.010
65165	5489	21	4.61	0.117	+0.00	0.086	−0.07	5388	58	4.41	0.018	−0.05	0.015
65352	5344	30	4.57	0.065	−0.27	0.013	−0.34	5179	37	4.29	0.016	−0.38	0.010
65355	5171	94	4.59	0.103	−0.26	0.033	−0.33	5026	49	4.34	0.018	−0.36	0.015
65935	5123	99	4.69	0.104	−0.01	0.068	−0.08	5058	36	4.59	0.010	−0.04	0.010
66509	5484	17	4.15	0.025	−0.63	0.094	−0.70	5595	65	4.35	0.014	−0.54	0.014
67211	4817	155	4.40	0.090	−0.30	0.045	−0.37	4867	32	4.49	0.010	−0.27	0.010
67282	5432	18	4.83	0.089	+0.00	0.043	−0.07	5217	38	4.43	0.016	−0.11	0.011
67773	5336	43	4.65	0.095	−0.20	0.030	−0.27	5203	52	4.44	0.016	−0.30	0.015
67904	5268	53	4.43	0.035	−0.29	0.022	−0.37	5566	35	4.22	0.078	−0.08	0.013
70253	5645	41	4.16	0.022	−0.54	0.066	−0.61	5745	66	4.33	0.016	−0.49	0.015
70319	5684	30	4.21	0.020	−0.32	0.009	−0.40	5729	37	4.26	0.007	−0.30	0.007
71720	5316	45	4.61	0.087	−0.06	0.052	−0.13	5121	51	4.31	0.022	−0.19	0.015

TABLE 6 — *Continued*

HIP	SMT3							SMT2					
	$T_{\rm eff}$ (K)	$\sigma(T_{\rm eff})$ (K)	$\log g$	$\sigma(\log g)$	[Fe/H]	σ([Fe/H])	[Fe/H]$_{\rm corr}$[a]	$T_{\rm eff}$ (K)	$\sigma(T_{\rm eff})$ (K)	$\log g$	$\sigma(\log g)$	[Fe/H]	σ([Fe/H])
72577	4965	107	4.67	0.090	−0.07	0.053	−0.15	4916	35	4.61	0.010	−0.11	0.010
72663	5591	37	4.31	0.046	−0.22	0.034	−0.29	5613	61	4.35	0.014	−0.20	0.014
72703	5682	51	4.68	0.128	−0.06	0.064	−0.13	5561	61	4.52	0.015	−0.14	0.014
73005	5236	73	4.39	0.055	−0.33	0.019	−0.40	5183	52	4.32	0.015	−0.36	0.013
73138	5382	45	4.64	0.162	+0.02	0.118	−0.05	5403	62	4.65	0.014	+0.04	0.014
73677	5673	44	4.12	0.028	−0.51	0.054	−0.59	5686	66	4.15	0.012	−0.51	0.012
73845	6456	249	4.46	0.089	+0.18	0.126	+0.10	5747	64	3.62	0.082	−0.39	0.036
74126	5689	57	4.59	0.110	−0.05	0.069	−0.12	5717	64	4.62	0.014	−0.04	0.014
74396	5269	97	4.81	0.209	+0.00	0.101	−0.07	5119	52	4.59	0.015	−0.09	0.015
75059	5754	64	4.34	0.041	−0.11	0.049	−0.18	5654	62	4.23	0.015	−0.16	0.014
75370	5485	15	4.19	0.024	−0.38	0.025	−0.45	5617	61	4.41	0.013	−0.28	0.015
75446	5561	27	4.53	0.085	−0.04	0.068	−0.11	5489	60	4.37	0.013	−0.08	0.013
75703	5582	34	4.81	0.168	−0.13	0.052	−0.20	5398	56	4.54	0.020	−0.26	0.015
76058	5818	50	4.55	0.047	−0.15	0.026	−0.23	5729	45	4.45	0.012	−0.21	0.011
76130	5863	87	4.36	0.045	−0.09	0.052	−0.16	5861	67	4.36	0.016	−0.10	0.015
76330	5237	69	4.81	0.140	+0.02	0.074	−0.06	5168	53	4.67	0.015	−0.02	0.015
76674	5476	16	4.79	0.146	+0.04	0.087	−0.03	5483	59	4.81	0.015	+0.04	0.015
77810	5860	108	4.57	0.108	+0.00	0.090	−0.07	5849	70	4.54	0.014	+0.00	0.013
78028	5791	100	4.31	0.051	−0.06	0.084	−0.13	5808	68	4.32	0.015	−0.05	0.015
78241	5393	44	4.49	0.106	−0.31	0.018	−0.39	5315	55	4.40	0.015	−0.38	0.015
78336	5131	136	4.83	0.212	+0.17	0.149	+0.09	5168	75	4.84	0.015	+0.19	0.015
78550	5612	37	4.40	0.067	−0.27	0.019	−0.34	5608	61	4.41	0.011	−0.28	0.011
78775	5336	61	4.39	0.069	−0.61	0.112	−0.68	5311	64	4.36	0.014	−0.62	0.014
78923	5685	70	4.35	0.067	−0.09	0.074	−0.17	5600	61	4.24	0.013	−0.14	0.011
79629	5645	30	4.34	0.031	−0.27	0.011	−0.34	5685	44	4.38	0.011	−0.24	0.011
80243	5353	40	4.65	0.140	+0.11	0.108	+0.04	5382	60	4.69	0.016	+0.13	0.013
80262	5624	29	4.60	0.084	−0.02	0.060	−0.10	5524	62	4.41	0.014	−0.09	0.014
81186	5199	56	4.76	0.094	−0.17	0.032	−0.24	5043	35	4.53	0.011	−0.27	0.011
81288	4929	156	4.44	0.085	−0.83	0.146	−0.91	4892	64	4.38	0.014	−0.86	0.013
81605	5602	32	4.58	0.095	−0.02	0.072	−0.09	5540	61	4.41	0.013	−0.06	0.013
81831	5635	44	4.60	0.125	−0.17	0.045	−0.24	5423	57	4.26	0.019	−0.33	0.016
82120	5564	16	4.29	0.023	−0.35	0.015	−0.42	5577	43	4.30	0.009	−0.34	0.009
82210	5807	111	4.60	0.146	−0.06	0.086	−0.14	5665	62	4.39	0.016	−0.13	0.014
82388	5693	159	4.08	0.107	−0.19	0.064	−0.26	6019	63	4.36	0.086	+0.38	0.019
82644	5828	105	4.59	0.126	−0.08	0.073	−0.15	5758	65	4.45	0.015	−0.12	0.015
82712	5595	25	4.47	0.064	−0.27	0.016	−0.34	5491	59	4.32	0.022	−0.35	0.015
83141	4884	144	4.61	0.110	−0.20	0.050	−0.27	4869	32	4.58	0.010	−0.21	0.010
83276	5820	52	4.00	0.044	−0.11	0.032	−0.18	5833	47	4.10	0.011	−0.10	0.011
83500	5852	88	4.17	0.027	−0.50	0.050	−0.58	5705	69	3.93	0.014	−0.60	0.014
84520	5820	80	4.39	0.063	−0.09	0.053	−0.16	5730	63	4.27	0.016	−0.14	0.014
85235	5382	31	4.44	0.060	−0.36	0.018	−0.43	5321	56	4.35	0.015	−0.39	0.015
85653	5439	22	4.37	0.052	−0.32	0.013	−0.39	5387	57	4.29	0.016	−0.35	0.015
86568	5315	47	4.37	0.042	−0.33	0.013	−0.40	5395	40	4.49	0.012	−0.28	0.010
86765	5622	35	4.34	0.040	−0.19	0.031	−0.26	5642	62	4.37	0.014	−0.17	0.014
87089	5184	103	4.46	0.084	−0.28	0.025	−0.35	5258	53	4.56	0.016	−0.23	0.015
88166	5397	18	4.22	0.027	−0.74	0.064	−0.81	5416	46	4.25	0.010	−0.73	0.010
88972	5075	129	4.50	0.100	−0.12	0.060	−0.19	5112	51	4.56	0.015	−0.09	0.015
90355	5620	32	4.40	0.049	−0.11	0.046	−0.18	5580	60	4.34	0.014	−0.14	0.014
90415	4950	95	4.36	0.049	−0.45	0.030	−0.52	4906	28	4.25	0.007	−0.47	0.007
90708	5760	84	4.39	0.073	−0.06	0.079	−0.13	5751	65	4.38	0.015	−0.06	0.015
91364	5396	61	4.81	0.187	−0.12	0.063	−0.19	5127	51	4.36	0.024	−0.30	0.016
91381	5534	15	4.42	0.065	−0.34	0.016	−0.41	5456	58	4.30	0.016	−0.38	0.012
91438	5712	41	4.54	0.065	−0.13	0.035	−0.20	5681	62	4.45	0.030	−0.14	0.012
91605	5071	150	4.72	0.157	−0.20	0.064	−0.28	4925	47	4.45	0.028	−0.29	0.015
91614	5622	51	4.27	0.036	−0.27	0.017	−0.34	5540	60	4.13	0.014	−0.33	0.015
91905	5472	11	4.44	0.052	−0.22	0.018	−0.30	5368	40	4.32	0.012	−0.30	0.011
92388	5449	22	4.38	0.068	−0.40	0.039	−0.47	5426	58	4.37	0.013	−0.42	0.013
92569	5714	47	4.55	0.075	−0.12	0.040	−0.20	5595	60	4.34	0.016	−0.20	0.015
93195	5342	44	4.69	0.131	+0.04	0.087	−0.03	5273	56	4.62	0.014	+0.00	0.014
93731	5414	31	4.65	0.154	−0.04	0.085	−0.11	5315	56	4.52	0.017	−0.10	0.015
94582	5523	14	4.69	0.080	−0.07	0.039	−0.14	5310	39	4.37	0.012	−0.20	0.011
95727	5272	66	4.16	0.061	−0.30	0.162	−0.37	5288	38	3.47	0.256	−0.37	0.196
96100	5437	32	4.67	0.123	−0.07	0.061	−0.15	5276	54	4.39	0.016	−0.17	0.015
96344	5714	45	4.15	0.018	−0.52	0.047	−0.60	5546	47	3.85	0.015	−0.65	0.012
96634	5283	51	4.54	0.072	−0.10	0.043	−0.18	5329	40	4.60	0.010	−0.07	0.010
96735	5179	69	4.80	0.111	−0.05	0.048	−0.13	5122	36	4.66	0.011	−0.07	0.011
97640	5703	70	4.68	0.223	−1.26	0.224	−1.33	4996	79	3.99	0.055	−1.89	0.087
97668	5056	74	4.59	0.065	−0.11	0.035	−0.19	5023	35	4.58	0.010	−0.14	0.010
98288	5778	63	4.24	0.026	−0.27	0.011	−0.34	5780	46	4.23	0.011	−0.27	0.010
98413	5102	69	4.73	0.077	−0.12	0.035	−0.20	5027	35	4.60	0.013	−0.17	0.011
98559	5595	23	4.34	0.037	−0.08	0.046	−0.15	5575	43	4.32	0.008	−0.09	0.008
98677	5519	15	4.56	0.090	−0.24	0.021	−0.31	5389	56	4.34	0.015	−0.33	0.015
98792	5045	73	4.38	0.036	−0.57	0.045	−0.64	5062	32	4.40	0.008	−0.56	0.008
98965	5651	46	4.63	0.123	−0.11	0.053	−0.19	5474	58	4.34	0.017	−0.25	0.016
99355	5135	94	4.68	0.112	−0.16	0.047	−0.24	5035	49	4.55	0.014	−0.23	0.015

TABLE 6 — *Continued*

HIP	SMT3							SMT2					
	$T_{\rm eff}$ (K)	$\sigma(T_{\rm eff})$ (K)	$\log g$	$\sigma(\log g)$	[Fe/H]	σ([Fe/H])	$[{\rm Fe/H}]_{\rm corr}$[a]	$T_{\rm eff}$ (K)	$\sigma(T_{\rm eff})$ (K)	$\log g$	$\sigma(\log g)$	[Fe/H]	σ([Fe/H])
99774	5583	18	4.04	0.033	–0.77	0.075	–0.85	5727	51	4.24	0.014	–0.68	0.010
99965	5512	28	4.46	0.083	+0.09	0.102	+0.02	5455	65	4.38	0.015	+0.06	0.015
100259	5928	110	4.66	0.124	–0.07	0.063	–0.14	5793	65	4.40	0.016	–0.16	0.015
101579	4941	110	4.63	0.083	–0.04	0.054	–0.11	4936	37	4.63	0.009	–0.04	0.009
101997	5527	15	4.40	0.059	–0.21	0.030	–0.28	5473	58	4.35	0.014	–0.24	0.014
102290	5859	62	4.48	0.053	–0.03	0.048	–0.10	5899	50	4.45	0.010	+0.00	0.010
102521	5924	118	4.56	0.100	–0.05	0.070	–0.13	5833	66	4.41	0.020	–0.12	0.014
103611	5678	35	4.60	0.073	–0.07	0.043	–0.14	5646	45	4.59	0.009	–0.09	0.009
103895	5453	13	4.20	0.012	–0.45	0.038	–0.52	5519	42	4.34	0.013	–0.41	0.010
103896	5839	66	4.51	0.060	–0.08	0.043	–0.16	5772	45	4.39	0.011	–0.13	0.010
104375	5302	64	4.75	0.159	–0.23	0.025	–0.31	5042	50	4.28	0.034	–0.39	0.016
104733	5790	49	4.52	0.054	–0.13	0.030	–0.20	5709	45	4.43	0.010	–0.17	0.007
106231	4897	108	4.55	0.169	–0.99	0.113	–1.06	4546	46	4.39	0.013	–1.26	0.015
106949	5592	17	4.25	0.012	–0.46	0.028	–0.53	5628	45	4.28	0.010	–0.43	0.010
107038	5230	66	4.65	0.110	+0.01	0.071	–0.07	5143	54	4.56	0.015	–0.04	0.014
107700	5217	97	4.60	0.130	–0.13	0.058	–0.20	5100	50	4.40	0.016	–0.20	0.015
108774	5708	61	4.65	0.128	–0.07	0.066	–0.15	5561	60	4.38	0.015	–0.15	0.015
108947	5388	49	4.60	0.161	–0.03	0.104	–0.10	5315	57	4.54	0.016	–0.08	0.016
109310	5883	60	4.39	0.034	–0.09	0.034	–0.16	5827	46	4.35	0.011	–0.12	0.010
110508	5662	41	4.57	0.090	–0.09	0.050	–0.16	5542	60	4.33	0.017	–0.17	0.015
111883	5132	86	4.65	0.099	–0.20	0.033	–0.27	5019	34	4.45	0.020	–0.26	0.010
111888	5029	121	4.78	0.127	–0.15	0.058	–0.22	5021	49	4.77	0.015	–0.15	0.015
111977	5735	58	4.34	0.051	–0.43	0.035	–0.50	5687	65	4.29	0.015	–0.45	0.015
112245	5565	19	4.40	0.047	–0.12	0.041	–0.20	5454	57	4.29	0.015	–0.21	0.013
112870	4944	191	4.34	0.072	–0.63	0.118	–0.71	4974	57	4.39	0.015	–0.62	0.015
113231	5670	52	4.24	0.022	–0.32	0.014	–0.39	5675	63	4.27	0.014	–0.32	0.013
113884	5815	52	4.24	0.014	–0.25	0.013	–0.32	5785	38	4.17	0.008	–0.26	0.008
113989	5575	33	4.11	0.040	–0.46	0.059	–0.53	5669	64	4.24	0.013	–0.39	0.014
114340	5667	31	4.59	0.061	+0.01	0.047	–0.07	5705	47	4.65	0.010	+0.02	0.010
114385	5794	71	4.55	0.081	+0.06	0.086	–0.01	5771	65	4.41	0.013	+0.05	0.013
115194	5040	89	4.37	0.035	–0.61	0.061	–0.69	5218	40	4.62	0.011	–0.48	0.011
115411	5502	14	4.30	0.038	–0.33	0.015	–0.40	5623	61	4.54	0.021	–0.24	0.015
115445	5180	167	4.76	0.225	–0.10	0.086	–0.17	5004	48	4.42	0.046	–0.20	0.014
116005	5129	69	4.72	0.075	–0.02	0.046	–0.09	5117	31	4.69	0.009	–0.03	0.007
116410	5484	13	4.34	0.041	–0.31	0.013	–0.38	5399	57	4.21	0.016	–0.36	0.015
118207	5691	37	4.25	0.018	–0.27	0.012	–0.34	5697	45	4.23	0.009	–0.26	0.008
118251	5696	69	4.20	0.016	–0.40	0.039	–0.47	5677	64	4.18	0.014	–0.41	0.014
118278	5533	15	4.41	0.052	–0.07	0.057	–0.15	5460	59	4.27	0.012	–0.11	0.012

[a] Corrected to match the metallicity scale of VF05 (see text).

TABLE 7
δM_V, ΔM_V, AND LITHIUM EWS OF THE KPNO SAMPLE

	$B-V$						$V-K_s$		
			SMT3		MOOG				
HIP	δM_V (mag)	$\sigma(\delta M_V)$ (mag)	ΔM_V (mag)	$\sigma(\Delta M_V)$ (mag)	ΔM_V (mag)	$\sigma(\Delta M_V)$ (mag)	δM_V (mag)	$\sigma(\delta M_V)$ (mag)	W(Li) (mÅ)
1674	0.43	0.12	0.01	0.12	···	···	–0.93	0.09	···
4907	0.32	0.11	0.14	0.13	0.14	0.11	0.26	0.07	···
5313	0.77	0.15	0.45	0.15	0.48	0.15	0.51	0.13	80.20
5521	0.32	0.11	0.14	0.13	0.03	0.11	0.21	0.08	12.17
9172	0.28	0.12	0.12	0.14	0.12	0.12	···	···	69.40
9829	0.32	0.11	–0.06	0.11	0.10	0.11	0.14	0.06	···
10276	0.56	0.17	0.34	0.18	0.30	0.17	0.37	0.10	···
10629	0.32	0.13	–0.19	0.13	···	···	0.06	0.10	···
11507	0.43	0.18	0.22	0.18	···	···	0.22	0.11	···
12685	0.33	0.14	0.07	0.16	···	···	–0.07	0.12	75.40
13771	0.41	0.20	0.05	0.20	···	···	0.04	0.14	···
14241	0.46	0.17	–0.07	0.17	···	···	0.11	0.10	···
14300	0.25	0.13	–0.03	0.13	···	···	0.27	0.09	···
15062	0.56	0.13	0.14	0.13	···	···	0.24	0.10	32.50
15442	0.25	0.11	–0.01	0.12	–0.02	0.11	0.15	0.07	13.83
17265	0.60	0.16	–0.05	0.19	–0.02	0.16	0.23	0.09	···
18324	0.38	0.11	–0.13	0.12	–0.12	0.11	0.11	0.07	···
20722	0.23	0.13	0.10	0.17	···	···	0.13	0.10	24.90
21276	0.30	0.12	0.13	0.15	0.11	0.12	–0.10	0.08	74.30
21571	0.36	0.11	0.06	0.12	0.06	0.12	0.17	0.08	···
21832	0.50	0.11	–0.05	0.13	–0.10	0.12	0.01	0.08	···
22175	0.33	0.12	0.10	0.14	0.15	0.12	0.23	0.08	···
23431	0.37	0.14	–0.15	0.15	···	···	0.23	0.11	···
23786	0.30	0.11	0.10	0.12	0.03	0.11	0.05	0.08	···
26505	0.50	0.11	–0.02	0.11	–0.05	0.11	0.16	0.08	···
30862	0.53	0.11	–0.04	0.11	0.02	0.11	0.29	0.07	15.31
44259	0.58	0.21	0.18	0.21	···	···	0.15	0.09	···
44262	0.23	0.25	0.08	0.26	···	···	0.14	0.16	···
52278	0.28	0.12	–0.22	0.13	···	···	0.36	0.09	···
52470	0.42	0.11	–0.06	0.11	–0.01	0.11	0.31	0.08	···
54906	0.39	0.11	0.10	0.12	0.13	0.11	0.26	0.07	···
55210	0.33	0.11	0.08	0.11	–0.01	0.11	0.11	0.08	···
56092	0.44	0.24	0.11	0.25	···	···	0.47	0.15	···
56337	0.41	0.19	0.21	0.19	···	···	0.31	0.12	···
56837	0.58	0.13	0.18	0.13	···	···	···	···	···
57939	1.37	0.10	0.12	0.22	0.15	0.10	0.67	0.07	···
57992	0.63	0.11	0.22	0.11	0.23	0.11	0.34	0.07	···
58949	0.40	0.12	0.04	0.12	0.09	0.12	0.08	0.08	···
60074	0.29	0.11	0.10	0.12	0.14	0.11	0.17	0.06	125.50
60268	0.64	0.12	–0.07	0.13	0.10	0.12	0.08	0.08	···
63322	0.42	0.25	0.22	0.26	···	···	–0.34	0.16	121.40
63346	0.43	0.11	–0.09	0.12	0.01	0.11	0.12	0.07	···
63636	0.24	0.11	0.05	0.14	–0.01	0.11	0.24	0.07	25.55
64076	0.51	0.12	0.21	0.13	···	···	0.21	0.09	13.04
64131	0.64	0.14	–0.06	0.16	···	···	0.36	0.11	···
65165	0.25	0.11	0.09	0.14	0.10	0.12	0.22	0.08	···
65352	0.48	0.11	0.09	0.11	0.04	0.11	0.38	0.07	···
65355	0.34	0.11	–0.04	0.12	–0.05	0.12	0.30	0.08	···
65935	0.46	0.24	0.29	0.25	···	···	0.27	0.14	···
66509	0.49	0.20	–0.19	0.22	···	···	0.07	0.14	···
67211	0.49	0.27	0.08	0.28	···	···	0.18	0.13	···
67282	0.32	0.17	0.15	0.17	···	···	0.26	0.09	···
67773	0.43	0.13	0.10	0.13	···	···	0.19	0.09	···
67904	0.34	0.11	–0.07	0.12	–0.07	0.11	0.33	0.08	···
70253	0.60	0.12	–0.01	0.13	0.01	0.12	0.21	0.08	···
70319	0.42	0.10	–0.01	0.10	–0.00	0.10	0.04	0.06	···
71720	0.31	0.23	0.10	0.24	···	···	0.41	0.13	···
72577	0.41	0.23	0.18	0.24	···	···	0.20	0.14	···
72663	0.39	0.19	0.04	0.20	···	···	0.23	0.14	···
72703	0.39	0.17	0.17	0.18	···	···	0.30	0.09	87.00
73005	0.31	0.10	–0.13	0.11	–0.10	0.11	0.17	0.06	···
73138	0.58	0.19	0.43	0.23	0.47	0.19	0.28	0.14	···
73677	0.49	0.13	–0.10	0.14	···	···	0.34	0.11	···
73845	0.38	0.20	0.36	0.23	–0.16	0.20	0.16	0.14	···
74126	0.61	0.19	0.40	0.20	0.54	0.19	0.31	0.14	29.80
74396	0.32	0.11	0.16	0.15	0.08	0.12	0.12	0.08	···
75059	0.25	0.15	–0.01	0.16	···	···	0.35	0.13	···
75370	0.42	0.17	–0.06	0.17	···	···	–0.07	0.10	···
75446	0.53	0.19	0.33	0.20	0.36	0.19	0.41	0.13	···
75703	0.60	0.17	0.33	0.18	···	···	0.36	0.10	14.20
76058	0.47	0.19	0.17	0.20	···	···	0.24	0.13	18.60
76130	0.34	0.20	0.10	0.21	···	···	0.30	0.15	27.10

TABLE 7 — *Continued*

	$B-V$						$V-K_s$		
			SMT3		MOOG				
HIP	δM_V (mag)	$\sigma(\delta M_V)$ (mag)	ΔM_V (mag)	$\sigma(\Delta M_V)$ (mag)	ΔM_V (mag)	$\sigma(\Delta M_V)$ (mag)	δM_V (mag)	$\sigma(\delta M_V)$ (mag)	W(Li) (mÅ)
76330	0.43	0.12	0.28	0.14	0.13	0.12	0.16	0.09	···
76674	0.29	0.19	0.15	0.21	···	···	0.05	0.13	71.60
77810	0.43	0.15	0.27	0.18	···	···	0.43	0.13	120.60
78028	0.30	0.14	0.08	0.16	···	···	0.14	0.12	···
78241	0.55	0.11	0.13	0.11	0.13	0.11	0.26	0.07	···
78336	0.55	0.22	0.52	0.26	0.46	0.22	0.17	0.10	28.10
78550	0.62	0.14	0.23	0.14	···	···	0.28	0.11	···
78775	0.59	0.10	–0.08	0.15	–0.08	0.10	0.21	0.06	···
78923	0.23	0.13	–0.01	0.15	···	···	0.17	0.10	···
79629	0.47	0.11	0.08	0.11	0.13	0.11	0.05	0.07	···
80243	0.37	0.16	0.30	0.19	0.24	0.16	0.11	0.07	···
80262	0.30	0.13	0.12	0.14	···	···	0.11	0.10	···
81186	0.49	0.21	0.19	0.21	0.08	0.21	0.30	0.09	···
81288	0.57	0.16	–0.29	0.22	–0.23	0.16	0.11	0.09	···
81605	0.26	0.13	0.07	0.15	···	···	0.07	0.10	···
81831	0.64	0.18	0.34	0.19	0.29	0.19	0.64	0.12	···
82120	0.50	0.13	0.04	0.13	···	···	0.17	0.10	···
82210	0.33	0.12	0.11	0.15	···	···	0.35	0.09	14.20
82388	0.31	0.13	–0.01	0.14	···	···	0.25	0.10	128.70
82644	0.44	0.13	0.21	0.15	···	···	0.28	0.09	54.90
82712	0.48	0.13	0.10	0.13	···	···	0.13	0.10	···
83141	0.37	0.21	0.04	0.22	···	···	0.15	0.10	···
83276	0.35	0.13	0.09	0.13	···	···	0.14	0.10	15.54
83500	0.29	0.19	–0.29	0.19	···	···	0.32	0.12	32.30
84520	0.26	0.11	0.02	0.13	–0.03	0.12	0.25	0.08	14.20
85235	0.55	0.10	0.09	0.10	0.09	0.10	0.23	0.06	···
85653	0.24	0.10	–0.19	0.11	–0.20	0.11	–0.03	0.07	···
86568	0.66	0.28	0.23	0.28	···	···	0.27	0.15	···
86765	0.38	0.11	0.06	0.12	0.11	0.12	0.14	0.09	···
87089	0.48	0.17	0.08	0.18	···	···	+0.00	0.10	···
88166	0.74	0.21	–0.03	0.22	···	···	0.35	0.15	···
88972	0.31	0.10	0.05	0.12	–0.03	0.11	0.01	0.06	···
90355	0.51	0.13	0.26	0.14	···	···	0.17	0.11	···
90415	0.36	0.27	–0.17	0.27	···	···	0.29	0.13	···
90708	0.31	0.19	0.10	0.21	···	···	0.25	0.13	···
91364	0.33	0.11	0.07	0.13	–0.07	0.11	0.15	0.07	···
91381	0.43	0.13	–0.01	0.13	···	···	0.17	0.10	···
91438	0.44	0.10	0.17	0.11	0.14	0.10	···	···	···
91605	0.57	0.16	0.24	0.17	0.10	0.16	0.23	0.08	···
91614	0.27	0.19	–0.12	0.19	···	···	0.24	0.14	···
91905	0.46	0.16	0.11	0.16	0.07	0.16	0.28	0.07	···
92388	0.61	0.17	0.12	0.17	···	···	0.20	0.09	···
92569	0.28	0.11	0.01	0.12	0.01	0.11	0.11	0.07	···
93195	0.28	0.12	0.15	0.15	0.09	0.12	0.13	0.09	···
93731	0.53	0.12	0.33	0.15	···	···	0.35	0.09	···
94582	0.36	0.22	0.14	0.22	···	···	0.31	0.10	···
95727	0.48	0.20	0.07	0.26	···	···	0.27	0.15	···
96100	0.35	0.10	0.12	0.12	0.07	0.11	···	···	···
96344	0.38	0.28	–0.21	0.29	···	···	0.51	0.15	···
96634	0.35	0.17	0.10	0.18	···	···	–0.01	0.10	···
96735	0.41	0.17	0.20	0.18	···	···	0.04	0.09	···
97640	0.29	0.11	–0.91	0.25	···	···	–0.37	0.07	···
97668	0.71	0.43	0.45	0.43	0.43	0.43	0.40	0.19	···
98288	0.29	0.19	–0.10	0.19	···	···	–0.04	0.13	19.30
98413	0.41	0.19	0.15	0.19	···	···	0.09	0.13	···
98559	0.42	0.21	0.19	0.21	···	···	0.18	0.15	···
98677	0.51	0.11	0.14	0.11	0.16	0.11	0.24	0.07	10.57
98792	0.55	0.10	–0.09	0.11	–0.08	0.10	0.13	0.07	···
98965	0.47	0.15	0.21	0.16	···	···	0.28	0.12	···
99355	0.54	0.16	0.24	0.17	0.09	0.16	0.26	0.08	···
99774	0.77	0.17	–0.04	0.19	···	···	0.32	0.10	···
99965	0.39	0.11	0.30	0.15	0.41	0.11	0.36	0.07	···
100259	0.31	0.13	0.09	0.14	···	···	–0.05	0.10	67.20
101579	0.40	0.17	0.20	0.18	···	···	0.08	0.09	···
101997	0.43	0.10	0.10	0.11	0.14	0.11	···	···	···
102290	0.36	0.19	0.17	0.20	···	···	0.34	0.13	92.35
102521	0.30	0.12	0.09	0.14	–0.03	0.12	0.16	0.08	41.60
103611	0.37	0.18	0.15	0.19	···	···	0.29	0.12	32.50
103895	0.65	0.18	0.11	0.19	···	···	0.25	0.12	···
103896	0.52	0.19	0.29	0.19	···	···	0.35	0.13	···
104375	0.35	0.16	–0.01	0.16	–0.04	0.16	0.18	0.07	···
104733	0.41	0.11	0.13	0.11	0.15	0.11	0.26	0.06	20.90
106231	0.83	0.21	–0.15	0.24	···	···	–0.02	0.09	···

TABLE 7 — *Continued*

HIP	$B-V$						$V-K_s$		W(Li)
			SMT3		MOOG				
	δM_V (mag)	$\sigma(\delta M_V)$ (mag)	ΔM_V (mag)	$\sigma(\Delta M_V)$ (mag)	ΔM_V (mag)	$\sigma(\Delta M_V)$ (mag)	δM_V (mag)	$\sigma(\delta M_V)$ (mag)	(mÅ)
106949	0.56	0.15	0.02	0.16	···	···	0.21	0.13	···
107038	0.30	0.11	0.13	0.13	0.07	0.11	0.14	0.07	7.36
107700	0.30	0.16	0.03	0.17	–0.03	0.17	0.07	0.09	···
108774	0.25	0.12	0.03	0.14	–0.00	0.12	0.26	0.08	81.60
108947	0.35	0.17	0.16	0.20	···	···	0.16	0.09	···
109310	0.30	0.15	0.06	0.15	···	···	0.36	0.13	48.95
110508	0.23	0.11	–0.01	0.12	0.02	0.11	0.22	0.08	···
111883	0.37	0.16	0.04	0.17	–0.04	0.17	0.14	0.09	···
111888	0.55	0.16	0.26	0.17	0.17	0.16	0.11	0.07	···
111977	0.44	0.11	–0.07	0.11	–0.05	0.11	0.11	0.06	···
112245	0.30	0.11	0.03	0.11	0.04	0.11	0.11	0.07	···
112870	0.77	0.11	0.09	0.16	0.12	0.12	0.40	0.08	···
113231	0.41	0.14	–0.02	0.14	···	···	0.08	0.11	13.05
113884	0.55	0.16	0.19	0.16	···	···	0.24	0.13	21.17
113989	0.42	0.11	–0.13	0.12	–0.11	0.11	–0.08	0.06	···
114340	0.33	0.20	0.17	0.20	···	···	0.30	0.14	33.60
114385	0.38	0.16	0.27	0.18	···	···	0.56	0.13	105.80
115194	0.79	0.17	0.11	0.18	···	···	0.20	0.09	···
115411	0.63	0.18	0.19	0.18	···	···	–0.03	0.12	···
115445	0.35	0.16	0.10	0.18	–0.03	0.16	0.16	0.07	···
116005	0.38	0.11	0.20	0.12	0.10	0.11	0.05	0.08	···
116410	0.32	0.19	–0.10	0.19	···	···	0.17	0.12	···
118207	0.41	0.12	0.03	0.12	0.10	0.12	0.34	0.09	18.60
118251	0.32	0.12	–0.17	0.12	–0.14	0.12	0.16	0.08	···
118278	0.25	0.11	0.02	0.12	0.03	0.11	0.08	0.09	···